Universidade do Minho
Escola de Engenharia

Inês Araújo Parente

Development of a new Colon-Host simulator

Optimization of the cell-based module

janeiro de 2021

Development of a new Colon-Host simulator
Optimization of the cell-based module
Inês Araújo Parente
UMinho | 2021

ColOsH

MICRODIGEST

COMPETE 2020

PORTUGAL 2020

FCT
Fundação para a Ciência e a Tecnologia
MINISTÉRIO DA CIÊNCIA, TECNOLOGIA E ENSINO SUPERIOR

Universidade do Minho
Escola de Engenharia

Inês Araújo Parente

Development of a new Colon-Host simulator

Optimization of the cell-based module

Dissertação de Mestrado
Mestrado em Biotecnologia

Trabalho efetuado sob a orientação da
Doutora Clarisse Nobre
Doutora Cláudia Botelho
Doutora Catarina Gonçalves

janeiro de 2021

Acknowledgements

First of all, I would like to thank my supervisors Dr. Clarisse Nobre, Dr. Cláudia Botelho and Dr. Catarina Gonçalves who have given me the chance to be a part of their incredible projects and, for their consistent guidance and support throughout this work. I would like to thank the opportunity to learn and to work with them.

Furthermore, I would like to thank Dr. Miguel Xavier who took his time to discuss and enrich my work and, to guide me through the practical work always, with a word of encouragement. I would also like to thank Dr. Paulo Berni for all his comments and recommendations on this dissertation and, Dalila Roupar who has given me valuable support in the beginning of this work.

I am also thankful to the members of the Food Processing Group at INL who have given me a great deal of help and a truly good time in the lab. I would also like to thank Mafalda, Marisol, Patrícia and Yolanda for their support when things would get discouraging and for the fun moments we lived together.

A very special word goes to my parents who set me on this road and supported me unconditionally. I would like to thank my family and friends for their continuous encouragement over the years. I also wish to thank my nephews, Martim and Afonso, for reminding me what is really important in life and to always have fun.

The last words go to my partner Pedro without whom it would be impossible to complete this work.

This work was carried out at the Centre of Biological Engineering (CEB) at the University of Minho in collaboration with the International Iberian Nanotechnology Laboratory (INL). It was supported by the Fundação para a Ciência e Tecnologia (FCT) under the scope of the Project ColOsH (POCI-01-0145-FEDER-030071). It was also supported by the MICRODIGEST project (grant agreement 037716) co-funded by FCT and ERDF through COMPETE2020.

STATEMENT OF INTEGRITY

I hereby declare having conducted this academic work with integrity. I confirm that I have not used plagiarism or any form of undue use of information or falsification of results along the process leading to its elaboration.

I further declare that I have fully acknowledged the Code of Ethical Conduct of the University of Minho.

Desenvolvimento de um novo simulador Colon-Hospedeiro - Otimização do módulo celular

Resumo

A natureza dinâmica e composição única do intestino são difíceis de simular levando a um conhecimento limitado sobre as interações microbiota-hospedeiro. Vários modelos gastrointestinais *in vitro* têm vindo a ser desenvolvidos, contudo aspetos como a estabilidade do ecossistema microbiano ou das células do hospedeiro necessitam ser melhorados. O modelo ColOsH está a ser desenvolvido para solucionar as limitações dos modelos existentes. O ColOsH contém um módulo específico para a cultura de células intestinais - o Colon-Host, no qual será estudada a interação entre a microbiota e as células intestinais.

O presente trabalho visa otimizar o módulo celular para que, no futuro, as metodologias aqui estabelecidas possam ser transpostas para o Colon-Host. O modelo de cultura celular Caco-2/HT29-MTX foi usado e a resposta do epitélio intestinal aos produtos da fermentação de prebióticos pela microbiota humana foi estudada. Com a finalidade de estudar o seu efeito prebiótico, frutoligossacarídeos (FOS) e raftilose, foram usados como fontes de carbono para o crescimento da microbiota de fezes humanas.

O efeito dos produtos obtidos durante a fermentação foi estudado na viabilidade celular, produção de espécies reativas de oxigênio, permeabilidade intestinal, resistência elétrica transepitelial e expressão de proteínas específicas das *tight junctions* (microscopia confocal de varrimento a laser) da co-cultura Caco-2/HT29-MTX. A resposta inflamatória foi investigada através da quantificação da secreção da citocina IL-8 por ELISA e da expressão de genes pró-inflamatórios (*IL1B*, *IL6*, *CXCL8*, *TNF* e *PTGS2*) por qRT -PCR.

Inicialmente, os resultados demonstraram que o efeito dos produtos da fermentação na atividade metabólica de células Caco-2 é dependente da concentração de metabolitos e do tempo de fermentação. A otimização destes parâmetros permitiu garantir a viabilidade das células Caco-2 e da co-cultura Caco-2/HT29-MTX estabelecendo as condições padrão para os ensaios posteriores. Os produtos resultantes da fermentação demonstraram não comprometer a integridade da barreira da co-cultura Caco-2/HT29-MTX e as amostras das fermentações conduzidas em meio enriquecido com FOS revelaram ter um efeito antioxidante. Por fim, as amostras testadas não promoveram uma resposta inflamatória significativa.

Este trabalho permitiu otimizar os parâmetros do módulo celular do simulador Colon-Host com uma melhor representação do epitélio intestinal.

Palavras-chave: Caco-2/HT29-MTX co-cultura; interações colon-hospedeiro; microbiota intestinal; modelos intestinais *in vitro*;

Development of a new Colon-Host simulator - Optimization of the cell-based module

Abstract

The dynamic nature and the unique composition of the gut is difficult to simulate leading to a limited understanding of the microbiota-host interactions. Several *in vitro* gastrointestinal models have been developed over the years however, aspects need to be improved such as the stability of the ecosystem of microbial and host cells. The ColOsH model is being developed to solve the limitations of the existing models. The ColOsH contains a specific module for the culture of intestinal cells – the Colon-Host, in which the interaction between the gut microbiota and intestinal cells will be studied.

The present work aims to optimize the cell-based module so that in the future, the methodologies established here can be transposed to the Colon-Host. The Caco-2/HT29-MTX cell culture model was used and the response of the intestinal *in vitro* epithelium to products of the prebiotic fermentation by the human microbiota was studied. With the goal to study their prebiotic effect, fructo-oligosaccharides (FOS) and raftilose were used as carbon sources for the growth of the microbiota present in human faeces.

The effect of the fermentation products was studied on the cell viability, production of reactive oxygen species, intestinal permeability, transepithelial electrical resistance and expression of tight-junction specific proteins (imaged by laser scanning confocal microscopy) of the Caco-2/HT29-MTX co-culture. The inflammatory response was investigated by the quantification of the secretion of the IL-8 chemokine by ELISA and the expression of inflammatory response mediators' genes (*IL1B*, *IL6*, *CXCL8*, *TNF* and *PTGS2*) by qRT-PCR.

First results shown that the effect of fermentation products on the metabolic activity of Caco-2 cells was dependent on both concentration and incubation time. The optimization of these parameters ensured the viability of Caco-2 cells and Caco-2/HT29-MTX cells grown in co-culture, setting the standard conditions for the following experiments. Samples did not compromise the integrity of the intestinal barrier of the Caco-2/HT29-MTX co-culture and samples fermented with FOS-enriched media revealed a significant antioxidant effect. At last, the fermentation products tested did not promote a significant inflammatory response.

This work provided the optimization of several protocols and parameters allowing future tests to be performed in the Colon-Host simulator with a better representation of the intestinal epithelium.

Keywords: Caco-2/HT29-MTX co-culture; colon-host interactions; gut microbiota; intestinal *in vitro* models.

Contents

Abbreviations

ACTB: actin beta

COL: collagen

C_t: threshold cycle

CXCL8: C-X-C motif chemokine ligand 8

DAPI: 4′, 6-diamidino-2-phenylindole, dilactate

DCFH-DA: 2′,7′-dichlorofluorescin diacetate

DCF: dichlorofluorescein

DMEM: Dulbecco's modified Eagle's Medium

DMSO: Dimethyl sulfoxide

ECM: Extracellular matrix

FAO: Food and Agriculture Organization

FOS: Fructo-oligosaccharides

FM: Fermentative media

FBS: Foetal bovine serum

GPCRs: G protein-coupled receptors

GTI: Gastrointestinal tract

HBSS: Hank's balanced salt solution

HEPES: N-(2-Hydroxyethyl) piperazine-N′-(2-ethanesulfonic acid)

HMI®: Host Microbiota Interaction

HPLC: High performance liquid chromatography

HuMiX®: Human-Microbial Crosstalk

IL: interleukin

MAMP: Microbe-associated molecular patterns

MAPK: Mitogen-activated protein kinase

MAT: Matrigel

MEM: Minimum essential media

MTX: Methotrexate

NF-kB: nuclear factor-kappa B

PET: Polyethylene terephthalate

PFA: Paraformaldehyde

P-gp: P-glycoprotein

PRR: Pattern recognition receptors

qRT-PCR: quantitative reverse transcription polymerase chain reaction

ROS: reactive oxygen species

SCFA: short-chain fatty acids

SHIME®: Simulator of the Human Intestinal Microbial Ecosystem

TEER: Trans-epithelial electrical resistance

TIM®: TNO (gastro-) Intestinal Model

TLR: Toll-like receptors

TNF-α: Tumour necrosis factor alpha

List of figures

List of tables

Objectives and scope of the thesis

The current understanding of gut microbiota-host interactions is still limited. Due to the complexity of the gut, it is very hard to reproduce physiological conditions.

With the goal to solve the limitations of existing models, the ColOsH model is being developed at the Centre of Biological Engineering. The ColOsH is a modular reactor that comprises a module for the gut microbiota growth – the Colon-Reactor, and a module for the culture of intestinal cells – the Colon-Host, which will further allow microbiota-intestinal cells interaction studies.

The present work aims to conduct the first tests concerning the development of the Colon-Host simulator by optimizing the cell-based module. Studies were conducted to better understand the effect of prebiotic fermentation products produced by the microbiota present in primary human stool samples on a Caco-2/HT29-MTX co-culture.

In the future, the ultimate goal is to transpose the methodologies stablished in this work into the ColOsH model.

CHAPTER I. Introduction - The Human intestine

The human intestine is a dynamic and complex environment that undertakes many important roles including food digestion, nutrient absorption, protection against pathogenic agents, immune responses, among others[1,2]. It is divided into small and large intestine, each with very specific functions.

The small intestine is directly responsible for the digestion of proteins, fats and carbohydrates to smaller components, allowing their absorption[3,4]. In turn, the large intestine, also known as colon, processes food components that were not digested in the small intestine and also absorbs water, vitamins and electrolytes[5].

The human intestinal epithelium is formed by a single layer of columnar epithelial cells separating the intestinal lumen from the underlying lamina propria. It acts as a protective barrier from the harsh luminal environment. The intercellular space is sealed by tight junctions which regulate the permeability of the intestinal epithelium.

The physiology, structure and cell composition of the intestinal epithelium, in the small intestine and in the colon, are very different (**figure 1**).

The intestinal epithelium forms tubular invaginations called crypts. The small intestine epithelium extends over structures, called villi, which are projected into the lumen, however, these are not present in the colon that presents a relative flat surface. The presence of villi increases the surface area allowing a more efficient nutrient absorption. The luminal surface of colonocytes and enterocytes is covered with microvilli that increase the absorptive area and the uptake of nutrients, vitamins, ions and water[6].

Different cell lineages are found in the gut epithelium, each with unique functions. Enterocytes are the most prominent cell type of the intestinal epithelium being responsible for the metabolic and digestive functions. Secretory cells include goblet cells that secrete mucins, and Paneth cells that secrete antimicrobial factors. Enteroendocrine cells link the central and enteric neuroendocrine systems through the secretion of regulatory hormones linked to digestive functions. Finally, chemosensory tuft cells have an important role in defence against helminths while M cells present luminal antigens to the immune system[7,8].

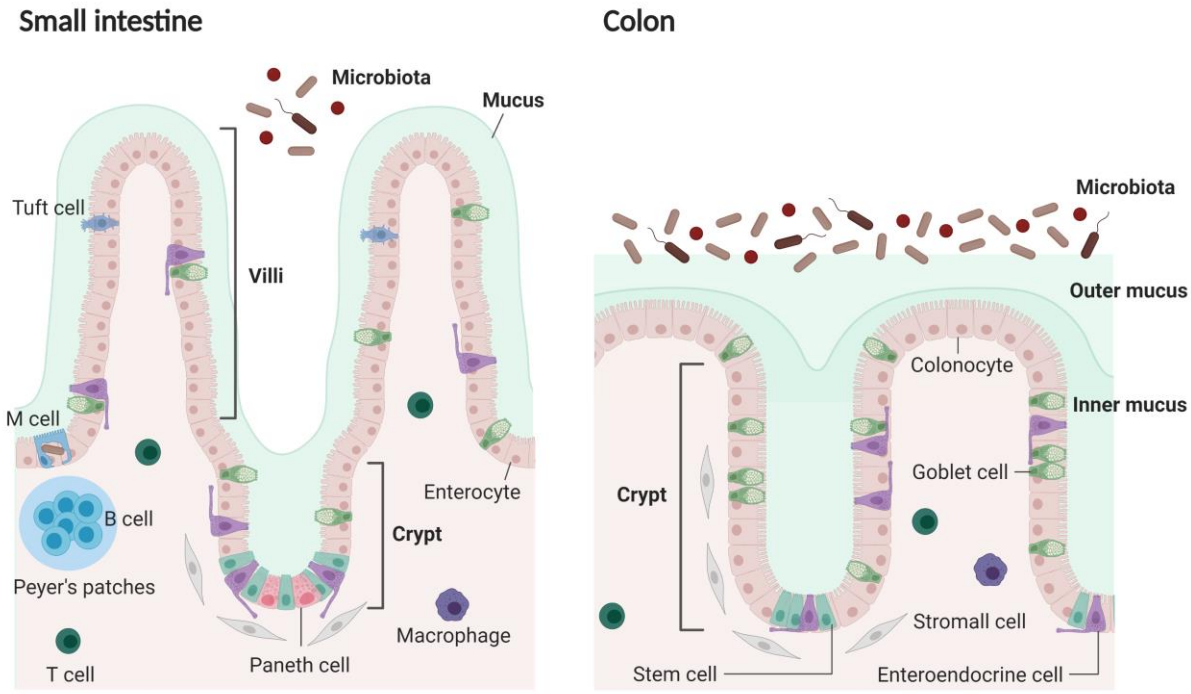

Figure 1: Schematic representation of the **intestinal epithelium A) small intestine and B) colon**. Adapted from Peterson *et al.* (2014). Created with BioRender.

At the base of these crypts reside intestinal stem cells that are responsible for regenerating all mature intestinal epithelial cells including enterocytes, enteroendocrine cells, goblet cells and Paneth cells. Stem cells give rise to proliferative cells that differentiate as they migrate up the crypt-villus axis leading to a constant renewal of the intestinal surface[7]. The migration and differentiation of cells along the crypts is controlled by gradients of growth factors, cytokines, products of microbial fermentation, food metabolites and gases along with alterations on physical properties underlying the extracellular matrix (ECM) such as stiffness and porosity[6].

Most of the nutrient transport occurs in the small intestine, whereas the colon is mainly responsible for water absorption and electrolyte transport. However, enzymes in the upper gastrointestinal tract (GIT) are unable to cleave more complex carbohydrates[9]. The undigested food that passes to the large intestine becomes available for fermentation by the colonic microbiota. The metabolites that result from this conversion are in close contact with enterocytes having, consequently, an effect on the host's metabolic phenotype[10].

I.1. Gut Microbiota

The complex and heterogeneous population of microorganisms that inhabits different parts of the human body is collectively known as microbiota[11,12]. In turn, the term microbiome refers to the collective genomes of the microorganisms in a particular environment[13]. In the last few decades, many efforts have been made to deep the current understanding of microbiota-host interactions. However, knowledge in this area is still limited due to methodologic challenges. To this day, primary human stool samples are the closest *in vivo* representation of the gut microbiota. Besides being impractical, the process of human stool sampling demands successful recruitment to ensure a representative statistical population. Acceptable collection methods, successful transport and processing of large quantity of data are imperative in large population-based studies[14,15].

Over 70% of the entire microbiota is located in the GIT[16]. Bacteria dominate the gut microbiota, but viruses, archea, fungi and other eukaryotes are also present[17]. The large intestine harbours the largest and most metabolically active microbial community[18]. It is predominantly inhabited by anaerobic bacteria that belong to the Firmicutes and Bacteriodetes phyla, but members of the Proteobacteria, Verrumicrobia and Actinobacteria phyla are also present[19,20].

In a recent study, *Forster et* al. showed differences in the functional role of each phylum[17]. They discovered that Firmicutes are dominated by uncharacterized functions however, spore formation, thiamine and riboflavin transport are all highly prominent. Many key specific functions of Bacteroidetes are identified including iron and sulphur transporter functions and specific sodium-transporting NADH:ubiquinone oxidoreductases. Proteobacteria display fructose bisphosphatase, glucokinases and regulators of iron cluster formation. Finally, prominent functions within the Actinobacteria are limited, but those identified were primarily associated with lipid and carbohydrate metabolism. This study demonstrated the distinct functions provided by the key phyla of the human gut microbiota. However, the prevalence of uncharacterized functions further demonstrates the need for better studies on this field.

The human gut microbiome is shaped by multiple host-endogenous and host-exogenous factors. It is believed that the environmental conditions have a substantially greater role than host genetics in shaping the human gut microbiome[21,22]. Recently, a study using data from 1,046 healthy individuals demonstrated that the host genetic background plays only a minor role in determining the microbiome composition as there was a lack of association with its genetic ancestry. The results further demonstrated that genetically unrelated individuals that share the same household have significant similarities in their microbiome and

that over 20% of the host-exogenous variability is associated with factors related to diet, drugs and/or anthropometry[22].

The intestinal microbiota works in tandem with the host's defences and the immune system to prevent pathogen colonisation and invasion. It also performs an essential role in the digestion process, breaking down complex carbohydrates, proteins, and some fats that reach the large intestine. The resultant metabolites can act locally or systemically, after absorption into the bloodstream[23]. Some examples are short-chain fatty acids (SCFA) and alcohols derived from monosaccharides, ammonia, branched-chain fatty acids, amines, sulphur compounds, phenols and indoles derived from amino acids and glycerol and choline derivatives derived from the breakdown of lipids[10].

SCFA mainly acetic, propionic, and butyric acids, are the main products of bacterial fermentation of undigested carbohydrates and proteins in the intestine. SCFA are normally absorbed in the colon and are either locally used as fuel for the colonic epithelial cells or enter into the bloodstream[24]. The rate, amount and type of SCFA produced depends on the species and amount of microorganisms in the colon, the substrate source, the colonic pH and the gut transit time[25].

Butyrate is considered the most important SCFA to maintain colonic health. Butyrate is the primary energy source of colonocytes and maintains intestinal homeostasis through anti-inflammatory actions[26]. This SCFA is almost completely metabolized by colonocytes and therefore is found in small amounts in peripheral blood[27]. Acetate, which is formed in higher quantities than other SCFA, is rapidly absorbed in the proximal colon and transported to the liver, where it can be used as a substrate for the synthesis of cholesterol. It also plays an important role regulating appetite[27,28]. About 90% of the propionate produced is transported to the liver, where it functions as a substrate for gluconeogenesis, lipogenesis, and protein synthesis[27,29].

Importantly, SCFA act not only as single components but also influence each other's production and function[27]. Figure 2 shows the schematic representation of SCFA production trough different carbohydrate fermentation pathways.

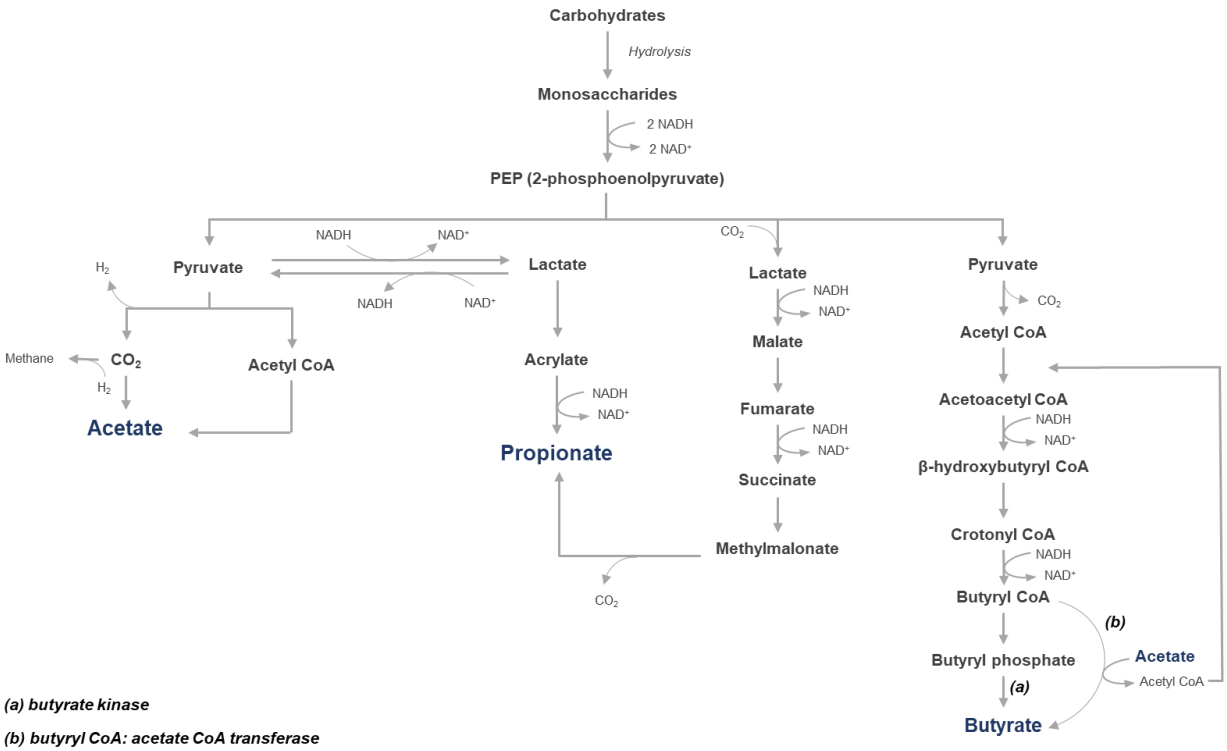

Figure 2: **Schematic representation of the production of acetate, propionate and butyrate** trough different carbohydrates fermentation pathways. Adapted from Venegas *et al.* (2019).

The normal functioning of the intestinal epithelial barrier is characterized by a homeostatic balance between the gut microbiota and host cells. This equilibrium is maintained by a community of obligate anaerobic bacteria, a thick mucus layer and the stimulation of the immune system. When this equilibrium is disturbed (dysbiosis) the community of microorganisms shifts from obligate to facultative anaerobic bacteria[30]. In a dysbiosis state, the mucus layer is decreased, and systemic inflammation is more likely to happen (**figure 3**)[8]. Systemic inflammation is characterized by an increase in mediators of the inflammatory response such as the tumour necrosis factor alpha (TNF-α) cytokine, and interleukins (IL)-6 and (IL)-8. During this process, microorganisms and metabolites from bacterial fermentation can escape the intestinal lumen and enter the blood stream due to a higher intestinal permeability.

Limiting the oxygen availability in the colon helps the host to ensure that the microbiota community is mostly composed by obligate anaerobe bacteria, benefiting the health of the host. The host maintains colonic epithelial cells (colonocytes) in a state of hypoxia (< 1% oxygen) ensuring a dominance of obligate anaerobic bacteria in the colon without restricting diversity of the microbiota[31].

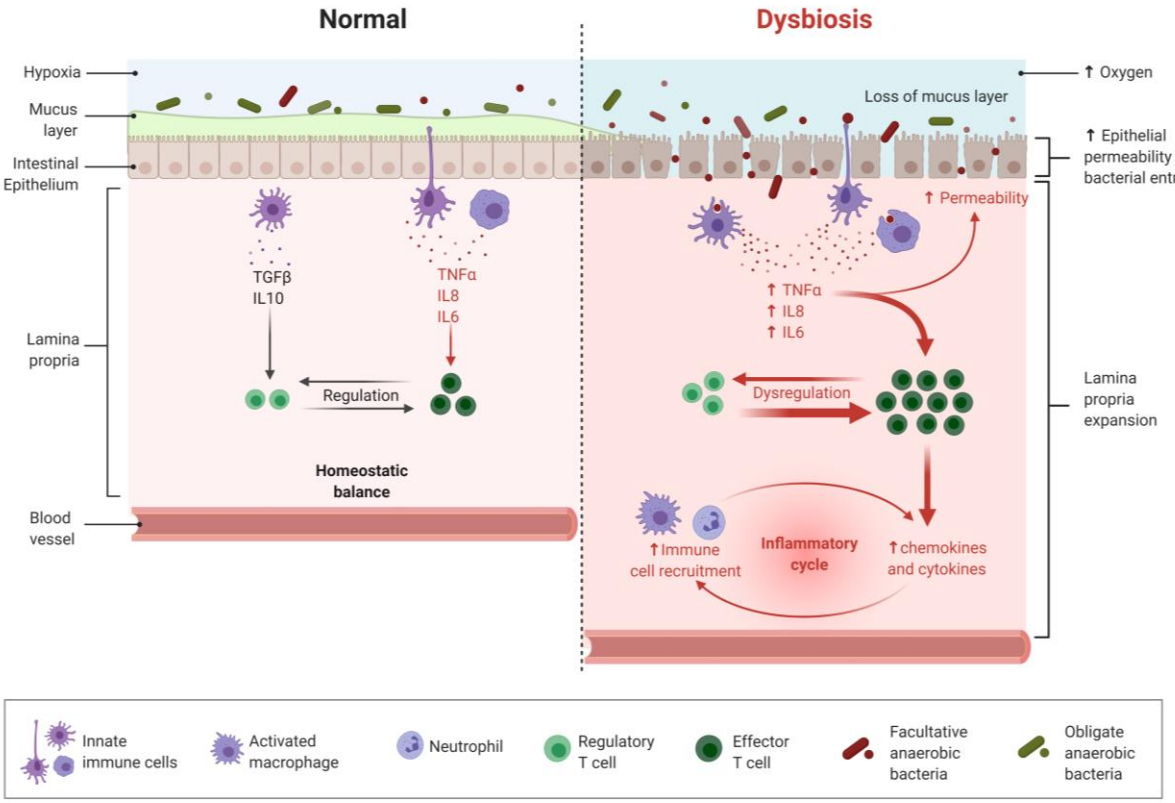

Figure 3: Schematic representation of **healthy intestinal barrier vs dysbiosis**. Adapted from Mu *et al.* (2017). Created with BioRender.

Over the past century, the number of individuals affected by multifactorial diseases such as autoimmune and neurodegenerative diseases, diabetes, obesity and allergies has significantly increased. Many of these diseases have been associated with dysbiosis[32]. However, many questions remain - namely whether dysbiosis is the cause or consequence of these pathologies[33]. The pathologies associated with dysbiosis are often associated with impaired intestinal barrier integrity leading to an increased intestinal permeability, which is commonly termed 'leaky gut' (**figure 4**)[34]. A leaky gut allows microorganisms and products from bacterial fermentation to enter the bloodstream, promoting both local and systemic inflammation.

Many environmental factors such as diet, genetics, hygiene, infections and medication are known to promote the establishment of a leaky gut state. There have been many attempts in preventing the leaky gut state. One of the most notorious being the daily intake of probiotic and prebiotic supplements.

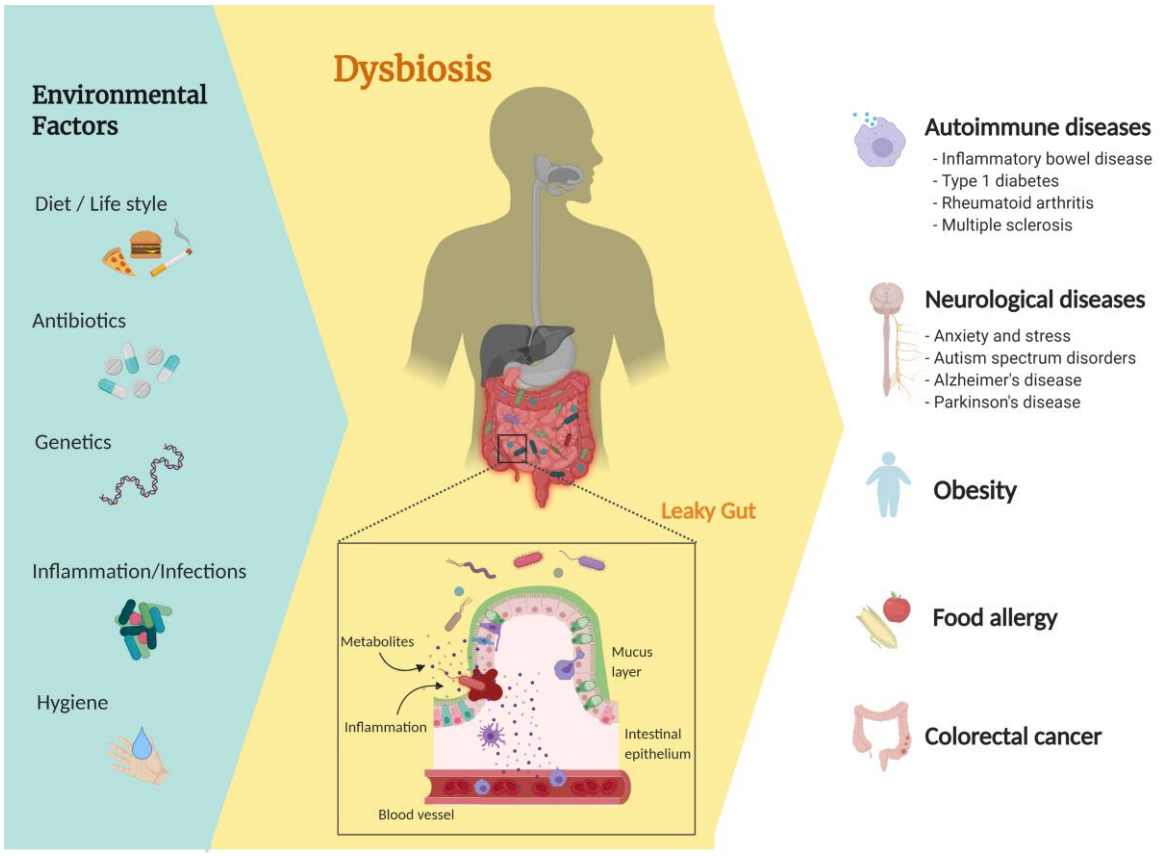

Figure 4: **Pathologies and environmental factors associated with a 'leaky gut'**. Created with BioRender.

I.1.1. Probiotics and prebiotics

For decades, the effect of probiotics on human health has been studied by both academia and industry (food and pharmaceutical)[35].

In 2001, an expert consultation of international scientists working on behalf of the Food and Agriculture Organization (FAO) of the United Nations and the World Health Organization (WHO) debated the emerging field of probiotics and defined probiotics as: "live microorganisms which when administered in adequate amounts confer health benefits on the host"[36,37]. Probiotics include bacterial species that interact with various cellular components within the intestinal environment. The interaction can be mediated by viable bacteria or by cellular components (such as the cell wall) or secreted molecules[38].

There are several mechanisms related with the health benefits provided by probiotics including immunomodulation, protection against physiological stress, suppression of pathogens, microbiota modulation and improvement of the gut barrier function[35]. The suppression of pathogens can be caused by a direct action of probiotics, through the enhancement of the intestinal epithelial barrier or by the

modulation of immune responses[39]. The epithelial barrier function can be enhanced by the modulation of signalling pathways, such as nuclear factor-kappa B (NF-kB), and mitogen-activated protein kinase (MAPK)- or Akt-dependent pathways, which lead to the induction of mucus production or increase tight junction functioning.

Most probiotic strains can also modulate host immune responses exerting local or systemic strain-specific effects. Many of the interactions between probiotic bacteria and intestinal epithelial immune cells are thought to be mediated by molecular structures, known as microbe-associated molecular patterns (MAMPs), which can be recognized through specific pattern recognition receptors (PRRs), such as toll-like receptors (TLRs)[40].

Microorganisms recognized as probiotics are generally from the *Lactobacillus* or *Bifidobacterium* genus. Most probiotics studied today belong to the Gram-positive lactic-acid bacteria group, in which the cell wall is typically composed by a thick peptidoglycan layer with proteins, teichoic acids and polysaccharides[39].

The concept of prebiotics has been changing since 1995, when it was firstly introduced by Gibson and Roberfroid[41]. Prebiotics were first defined as 'non-digestible food ingredients that beneficially affect the host by selectively stimulating the growth and/or activity of one or a limited number of bacteria in the colon, and thus improving host health'. However, a prebiotic effect has been attributed to many food components, sometimes without having all criteria in consideration[42]. In 2007, FAO/WHO experts described prebiotics as 'nonviable food components that confer health benefits to the host, associated with modulation of the microbiota'[43]. The most recent definition, published by the International Scientific Association for Probiotics and Prebiotics in 2017, defines prebiotic as 'a substrate that is selectively utilized by host microorganisms conferring a health benefit'[44].The consumption of prebiotics leads to numerous health benefits, affecting positively the development of beneficial intestinal bacteria, and are associated with a reduction of colorectal cancer and other tumours, a reduction of the risk of obesity and metabolic syndrome, an increased support of the immune system, and protection against infection[45]. Some examples of prebiotics include inulin, fructo-oligosaccharides (FOS), galacto-oligosaccharides, resistant starch, among others[46].

I.1.1.1. Fructo-oligosaccharides (FOS)

Fructo-oligosaccharides are one of the well-stablished prebiotics, which fulfil all criteria. FOS occur naturally in many plants, such as onion, chicory, garlic, asparagus, banana, artichoke, among others, contributing to their increasing popularity[47]. FOS are produced either by hydrolysis of inulin from plants or through the transfructosylation of sucrose by enzymes contained in a number of microorganisms, mainly fungi, particularly *Aureobasidium pullulans* (a yeast-like fungus), *Aspergillus* spp. and *Penicillium* spp.[48] (**figure 5**).

Structurally, FOS are non-conventional sugars, namely kestose (GF_2), nystose (GF_3) and fructofuranosylnystose (GF_4), composed by β(2 → 1)-linked fructose (F) units attached to a terminal glucose (G) moiety by a α(2 → 1) linkage (**figure 6**)[49].

FOS are not hydrolysed by the human digestive system but are selectively fermented by colonic microbiota, such as *Bifidobacterium* and *Lactobacillus* to form SCFA, inhibiting the growth of harmful microorganisms, stimulating the immune system, reducing liver toxins, and aiding in the absorption of certain minerals[50].

The ingestion of these prebiotics has been demonstrated to reduce inflammatory responses in pathologies such as irritable bowel syndrome[51], increase bone mineralization, density and structure[52], increase satiety[53] and regulate the immune system[54].

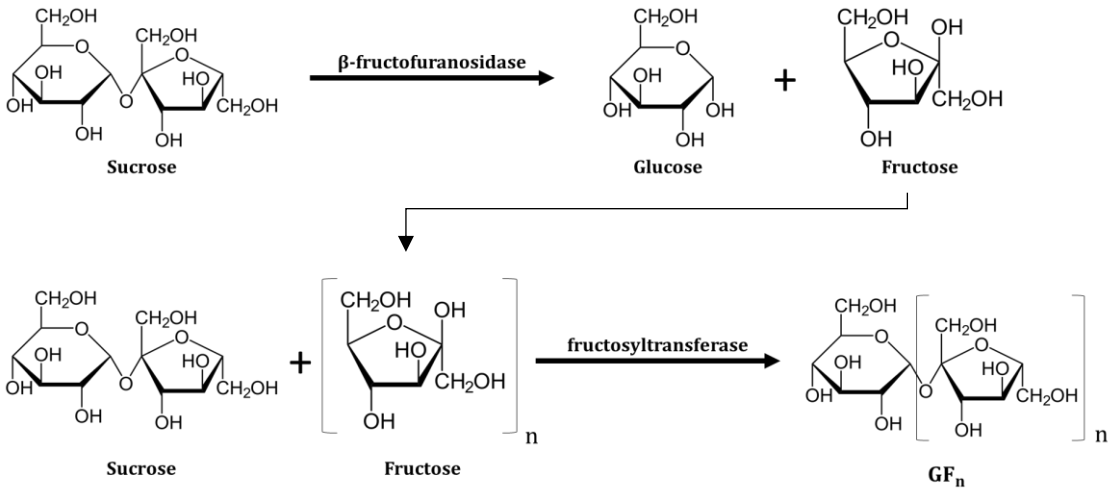

Figure 5: Synthesis of fructo-oligosaccharides (GF_n). (**A**) Hydrolysis of sucrose by β-fructofuranosidase into glucose and fructose. (**B**) Transfer of the fructosyl group by a fructosyltransferase enzyme to a sucrose molecule producing FOS.

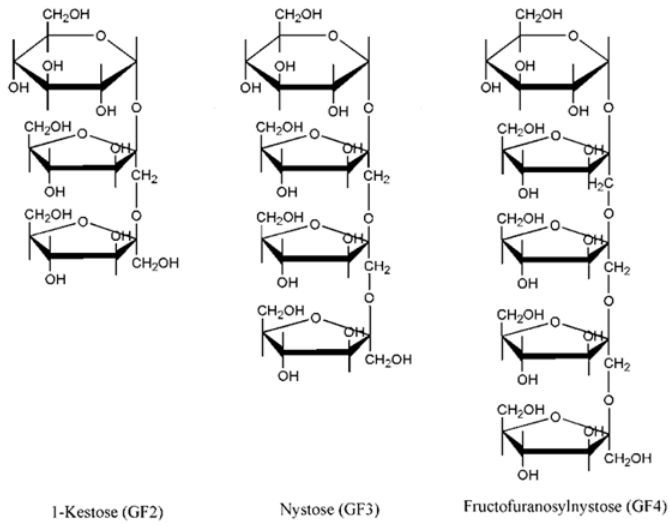

Figure 6: **Structure of fructo-oligosaccharides**: kestose (GF_2), nystose (GF_3) and fructofuranosylnystose (GF_4).

In this thesis, two different prebiotics were tested: a non-commercial microbial FOS, produced by *Aspergillus ibericus*, and raftilose, a commercial powder produced through enzymatic hydrolysis of chicory inulin. The prebiotic effect of FOS on a cell culture model was herein assessed and compared.

I.2. Intestinal *in vitro* models

The dynamic nature and the unique composition of the intestinal tract is difficult to simulate[55]. The significant breakthroughs in the intestinal research were possible due to the use of animal models. However, *in vivo* variables are difficult to control and predict. Animal models fail to resemble the human physiology, particularly in drug response studies, as the toxicity of certain compounds that are not toxic to humans may be so to animals and *vice versa*.

The use of *in vitro* models simplifies the study of the *in vivo* intestinal physiology and allows well-controlled and repeatable conditions for the evaluation of cellular responses[56]. Moreover, the costs and ethical issues associated with the use of animal experiments are significantly reduced using alternative *in vitro* models. Therefore, the study of the mechanisms involved in the microbiota-gut relationship requires reliable *in vitro* tools to recapitulate the human physiology allowing the improvement of the scientific knowledge and new therapeutics. The ideal *in vitro* model should recreate the essential features of the *in vivo* intestinal physiology and include: 1) all types of human-derived cells that represent the gut epithelium with the ability of being cultured for the defined assay time, 2) a 3D structure with similar properties to the lamina propria, 3) a fluidic system that provides physiological shear stress, adequate oxygenation and nutrients

to the cell medium, 4) a flexible substrate to provide cycle deformation to the epithelium, and finally 5) a close representation of the gut microbiota and of the epithelium/immune system crosstalk[55].

I.2.1. Cell-based *in vitro* models

2D cell models based on a single layer of cells (monolayer) growing on a porous membrane, represent a simplified tool to study interactions in a controlled manner, providing access to both sides: apical and basolateral. Most of them involve only one type of cell or tissue cultured in isolation. The human colorectal adenocarcinoma cell line Caco-2 (**figure 7**) is considered the standard model for the study of intestinal absorption of drugs. When in culture, Caco-2 cells grow towards a confluent monolayer and polarize, adopting morphological and functional characteristics of enterocytes. Polarized Caco-2 cells acquire an apical brush border with microvilli, form tight junctions between adjacent cells, and express enzymes typical of enterocytes (lactase, aminopeptidase N, sucrase-isomaltose and dipeptidyl peptidase)[57].

However, the mono-cellular Caco-2 model has several limitations given that the native intestinal epithelium is not composed only by enterocytes[58]. For example, due to an overexpression of tight junctions, the transepithelial electrical resistance (TEER), an indicator of epithelial barrier integrity, is much higher in Caco-2 when compared to the human intestine. In addition, the P-glycoprotein (P-gp) drug efflux is often overestimated and Caco-2 also lack the secretion of a mucous layer, which is an important constituent of the intestinal lumen[59].

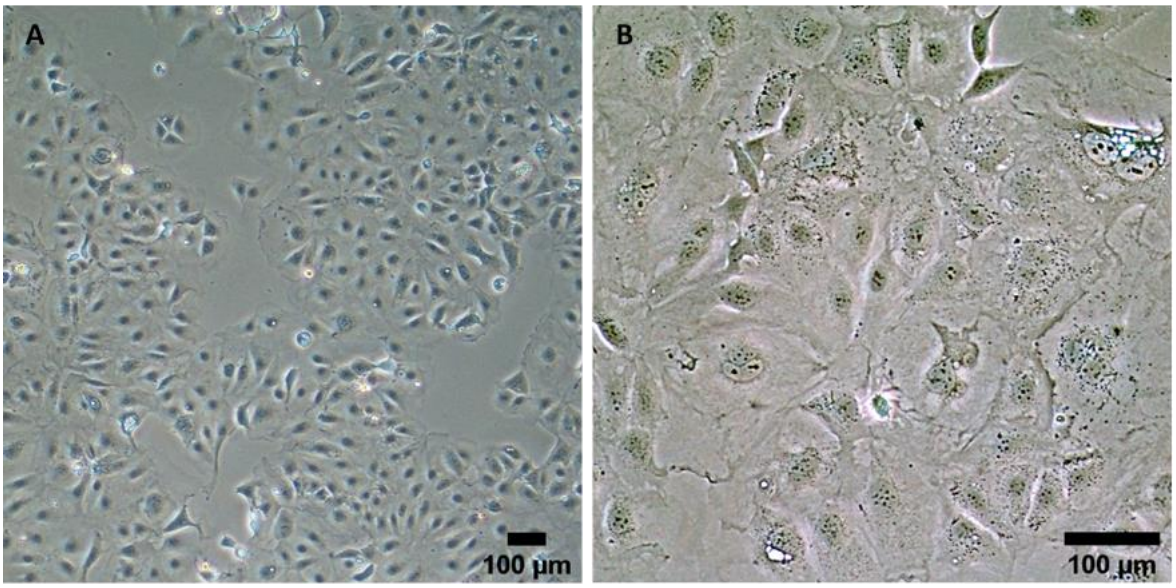

Figure 7: Optical microscopy images of **Caco-2 cells** at passage 36 grown in tissue culture flaks. A) 4x and B) 10x magnification.

Cell-based models using co-cultures of Caco-2 and mucus-producing cells were developed as a more complex and biologically relevant intestinal model. Also originating from human colonic adenocarcinoma, the HT-29 cell line can mimic goblet cells, the second major cell type of the intestinal epithelium. In 1990, Lesuffleur et al. established a stable homogeneous sub-population of mucus-secreting cells by treating HT-29 with methotrexate (MTX), giving rise to the HT29-MTX cell line, which grow in a monolayer of polarized goblet cells that produce a mucous layer (**figure 8**)[60].

Since the expression of tight junctions by HT29-MTX cells is inferior to Caco-2 cells, co-cultures of Caco-2/HT29-MTX in adequate ratios (typically 9:1) (**figure 9**) resemble more closely the *in vivo* scenario enabling an increased paracellular transport.

Co-culture and tri-culture models using Raji B cells have also been reported[61]. Raji B originated from a human Burkitt's lymphoma and have been reported to induce an M cell phenotype in Caco-2 cells. However, the phenotypes associated with these models are not fully characterized.

Cells are usually cultured on semi-permeable membranes in cell culture insert systems, which are the most commonly used to recreate an intestinal epithelial barrier *in vitro* and have been used to investigate intestinal lumen-to-blood permeability of various drugs and microorganisms (**figure 10**)[57]. Each insert divides a culture well in two compartments separated by a porous membrane. Typically, the apical side (top) corresponds to the intestinal lumen and the basolateral side represents the bloodstream. The membrane is made of a cell-culture compatible plastic and different pore sizes are commercially available. Cells are seeded directly on this membrane or coated with ECM-like coatings (e.g. Matrigel or hydrogels)[62].

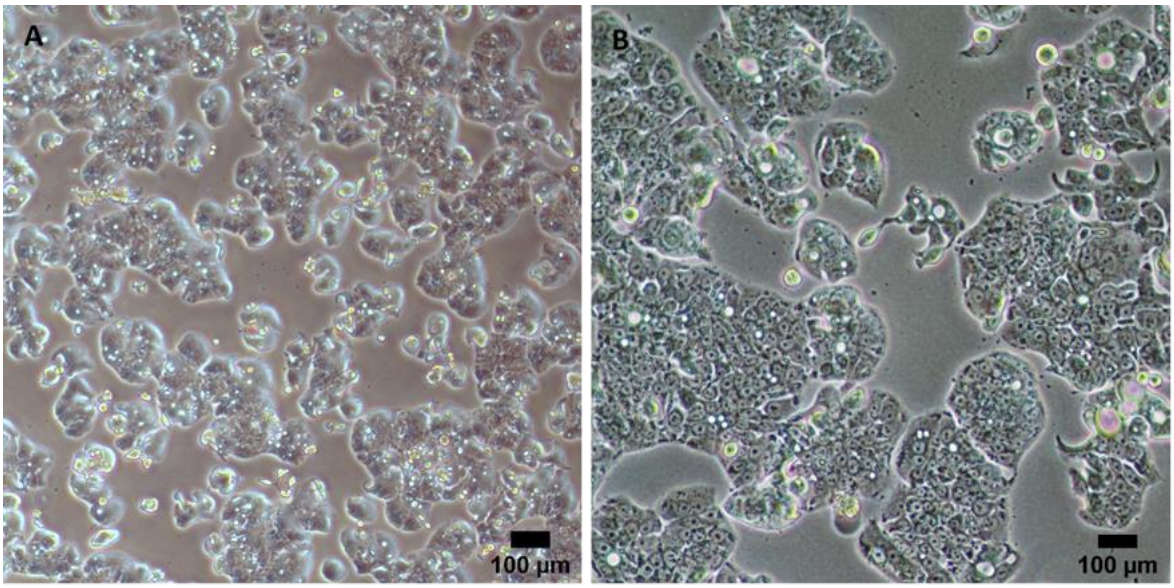

Figure 8: Optical microscopy image of **HT29-MTX cell line** at passage 65 grown in tissue culture flasks. A) 4x and a B) 10x magnification.

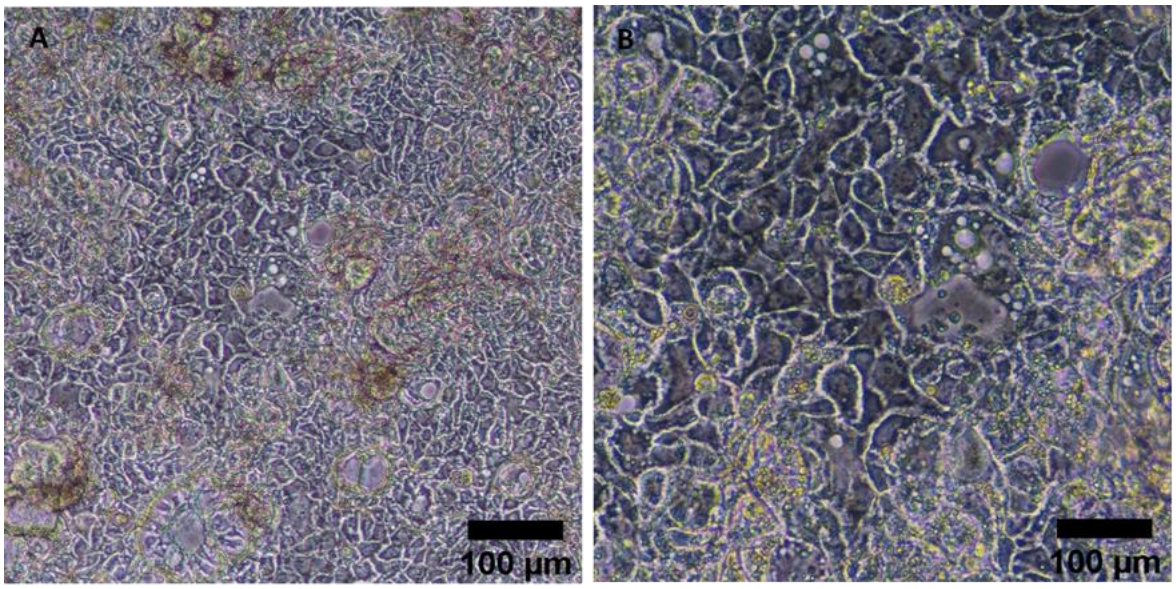

Figure 9: Optical microscopy image of **Caco-2/HT29-MTX co-culture** after 21 days of culture. A) 4x and 10x magnification.

Higher levels of cell differentiation have been achieved by 3D tissue models, using encapsulation of cells within hydrogels or organoid technology which is based on 3D clusters of primary or stem cells[63,64]. Despite their capacity to closer mimic the *in vivo* physiology, the static conditions lack vasculature hampers, continuous transport of signaling molecules and the removal of metabolic products from the tissue that can be toxic.

Organ-on-a-chip technology represents a potential approach to model multi-organ communication, based on three-dimensional cell cultures and microfluidic channels and chambers able to recreate the microphysiological environment. This technology offers the possibility to apply mechanical forces to mimic the physical microenvironment of living organs, such as peristaltic movements, and also the integration of sensors to monitor and even control of biological and physical parameters, such as pH, TEER, oxygen pressure, metabolites production, signal transmission[65].

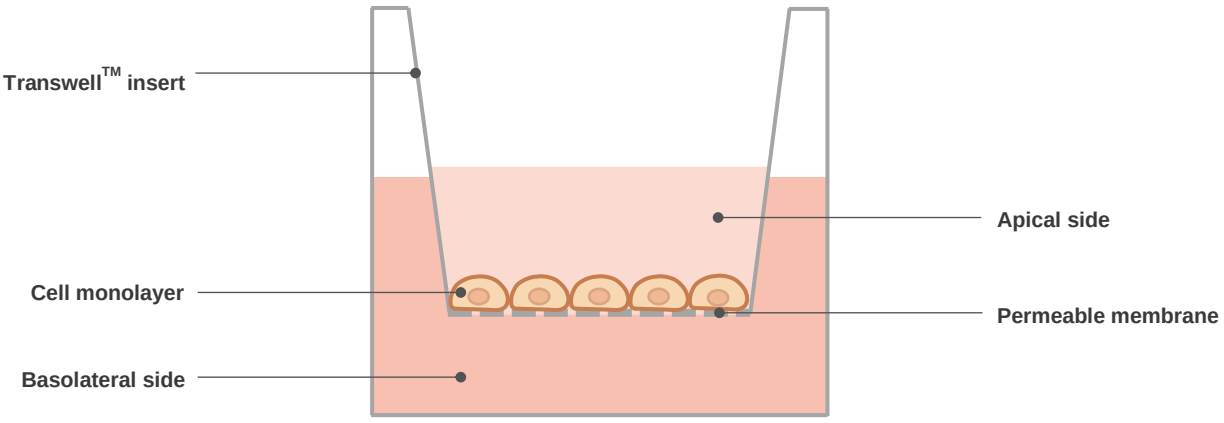

Figure 10: Schematic representation of a **cell culture insert system**.

I.2.2. Gastrointestinal fermentation models

The gut microbiota plays an important role not only on digestion but also on the immune response and the maintenance of the intestinal homeostatic balance. The study of these interactions *in vivo* is limited by ethical grounds, and *in vitro* by the challenge of emulate so complex physiological conditions[66].

In vitro intestinal fermentation models aim to study the interactions between the gut microbiota and host cells. Many models use faecal inoculum as a closer approximation to the intestinal ecosystem but most lack host interaction.

Batch fermentation is arguably the simplest (static) fermentation model. It uses closed anaerobic containers and short simulation times (**figure 11 A**). The digestion simulation in these static models ends when the substrate is depleted, and the accumulation of toxic metabolites disrupts the microbial balance. The culture conditions inside these containers, namely temperature, pH, anaerobiosis, and nutrition are controlled by a heating plate, alkali or acid dosing, N_2 bubbling and the supply of a basal medium, respectively. However, these systems have very limited resemblance to the *in vivo* conditions[67].

In turn, dynamic fermentation models allow longer digestion times being constantly fed by peristaltic pumps. Dynamic models are typically composed of multiple containers aligned in series to mimic the different digestive compartments. Each compartment has different physicochemical conditions according to its *in vivo* counterpart[67].

A pioneering example of a dynamic digestion system is the Simulator of the Human Intestinal Microbial Ecosystem - SHIME® (**figure 11 B**)[68]. In 1993, this five-stage reactor was developed to simulate the human gastrointestinal/microbial ecosystem[69,70]. Each reactor simulates a different part of the GIT: stomach, small intestine, ascending colon, transverse colon and descending colon. In this model, the 'intraluminal content' is continuously in transit, stirred and the pH automatically controlled. In addition, acids and the pancreatic juice are added to the stomach and small intestine reactors respectively, to more closely resemble the *in vivo* condition.

Later, a mucus layer has been integrated in the SHIME® model (M-SHIME®) that allows improved simulation of the mucosal and luminal microbiota in the GIT.

Another well-established model is the TNO (gastro-) Intestinal Model -TIM1 and TIM2 (**figure 11 C**). These automated models simulate the actions that occur along the GIT, including peristaltic mixing as well as the absorption of water and fermentation products. TIM1 simulates the stomach and the small intestine, whereas TIM2 mimics the large intestine[68,71]. The TIM® was designed to reproduce the conditions in the lumen of the gastro-intestinal tract by realistic mixing, transit of the meal, rate and composition of secretions and removal of digested products and water. It was also designed to predict the bioaccessibility of a wide variety of ingested compounds present in a broad range of foods and pharmaceutical matrices[72]. Water is pumped from a water bath into glass jackets surrounding flexible walls to control the temperature and pressure inside each compartment. Peristaltic movements are simulated by changes in the water pressure[73].

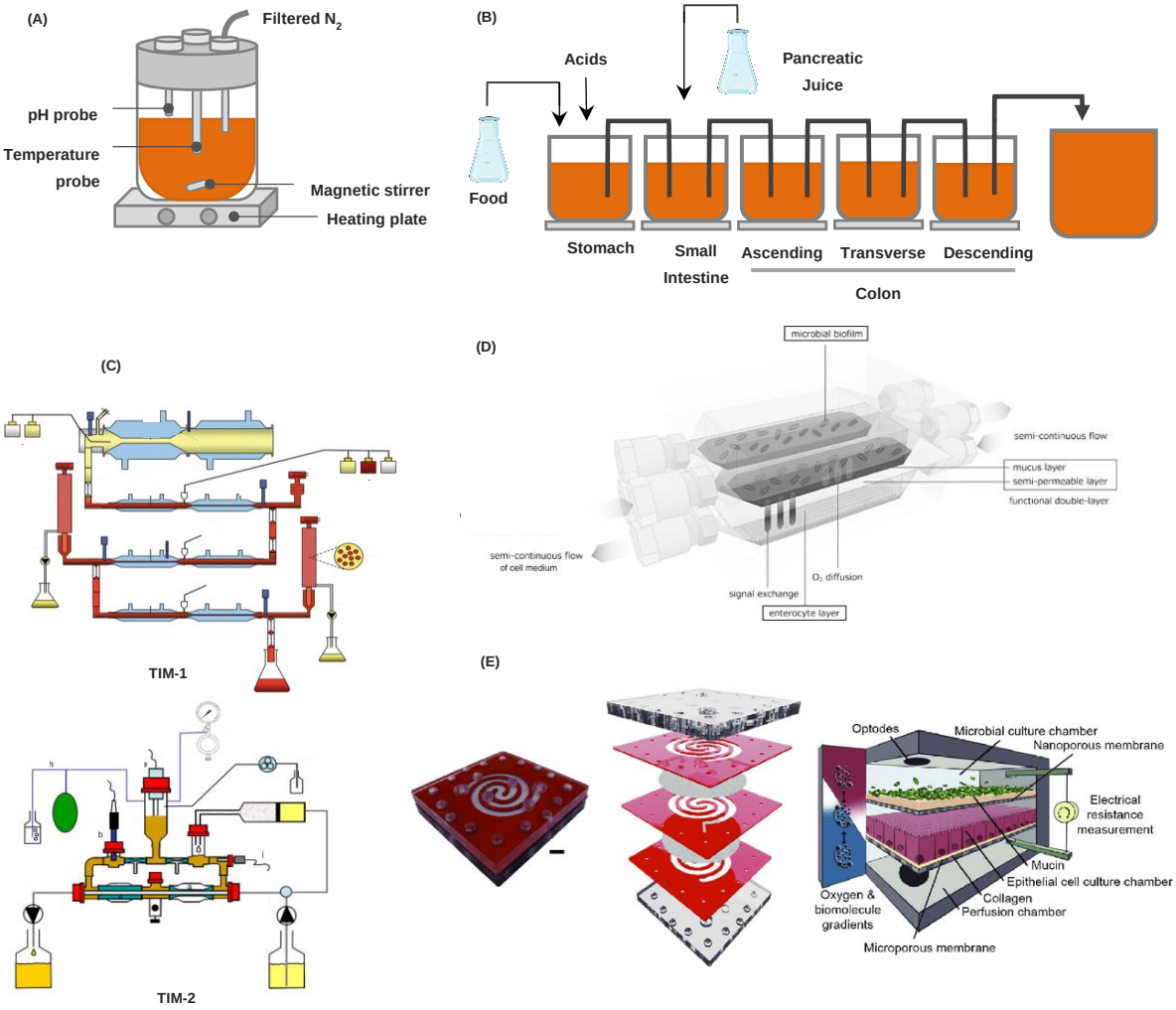

Figure 11: Schematic representation of **(A)** batch fermentation system **(B)** SHIME®. From Van de Wiele *et al.*, 2015. **(C)** TIM-1 and TIM-2. From Anson *et al.*, 2009 **(D)** HMI® from Marzorati *et al.*, 2014 **(E)** Humix®. From Shah *et al.*, 2018.

The HMI® (Host Microbiota Interaction) was developed to study the indirect host-microbe interaction in the GIT (**figure 11 D**). It is based on a co-culture system but in two separate compartments. The upper compartment simulates the luminal side of the GIT, whereas the lower compartment contains enterocytes, simulating the host. These two compartments have (semi-)continuous fluid flow and are separated by a functional double layer (a polyamide semi-permeable membrane and an artificial added mucus layer). The HMI® allows the study of bacterial adhesion under relevant shear forces and microaerophilic conditions. It also allows the reciprocal exchange of signals and metabolites between compartments and the exposure of cell lines to a complex microbial community, representative for the human colon[74].

The Human-Microbial Crosstalk (HuMiX®) device consists of three co-laminar microchannels: media perfusion, human epithelial cell culture and microbial culture (**figure 11 E**)[75]. Each chamber has dedicated inlets and outlets which allow the inoculation of the relevant cell lines and precise control over the physicochemical conditions within each microchamber through the perfusion of cell growth media[76]. Although HuMiX® was developed with a focus on host-microbe interactions, it may find applications in different industries, including pharmaceutic (drug screening, discovery and delivery) and food (nutritional studies). The ability to co-culture human and microbial cells in a controlled manner and to perform systematic investigations of such co-cultures opens numerous avenues for basic and applied research in the context of the human microbiota[76].

Altogether, these models have been used to i) examine roles of the GIT microbiota in the digestion of specific food ingredients[77], ii) understand the pharmacokinetics of drugs[78] and iii) model the gut microbiota linked to gastrointestinal disorders[79].

Numerous models have been developed over the last few years varying in complexity, reproducibility and versatility. Several aspects need to be reinforced and improved such as the stability of the microbial ecosystem or host cells over long-term experiments. In the future, multi-organ-chips can enclose the response of the several systems on a single device progressing to a simulation more similar to the *in vivo* conditions[67].

With the goal to solve the limitations of existing models the ColOsH model is being developed at the Centre of Biological Engineering at the University of Minho, under the ongoing Financed Project (PTDC/BTM-SAL/30071/2017). The ColOsH, which is currently under patent request, consists of a modular reactor comprising a module for microbiota growth – the Colon-Reactor, and a module for

intestinal cells culture – the Colon-Host, which will further allow microbiota-intestinal cells interaction studies. The Colon-Host module will include a co-culture of Caco-2/HT-29MTX cells in a semi-permeable membrane. To validate the system, the prebiotic effect of FOS (from microbial source) will be acessed in the ColOsH.

The present work aims to optimize the cell-based module so that in the future, the methodologies established here will be transposed to the Colon-Host simulator. A Caco-2/HT29-MTX cell culture model was used to evaluate the response of the intestinal epithelium to products of the prebiotic fermentation by the microbiota present in primary human stool samples.

CHAPTER II. Effect of human faecal fermentation products on an intestinal epithelium model based on Caco-2 cells

II.1. Quantification of SCFA produced in the prebiotic fermentation by the microbiota present in primary human stool samples

SCFA are the main products resulting from the fermentation of undigested carbohydrates by the microbiota present in the intestine[24]. To this day, primary human stool samples are the closest representation of the human gut microbiota.

Commercial Raftilose P95 or FOS produced by microorganisms in a previous work, were used as carbon sources for the microbiota growth (*in vitro* fermentation)[80].

In a previous work, human faecal samples from 5 healthy volunteers, were fermented in the presence of different carbon sources (FOS or Raftilose P95) for 24 h, under anaerobic conditions at 37 °C. Samples fermented with no carbon source were used as controls (data not published).

To perform the assays developed in the present work, the samples from the 5 fermentations were mixed to have a more representative sample. The SCFA profile obtained for samples collected at 12 and 24 h of fermentation, with the different carbon sources, is showed in **table 1**.

After 12 h of fermentation, Raftilose showed the highest SCFA concentrations except for n-butyrate. However, at the 24 h time-point, FOS showed higher concentrations of propionate and both iso and n-butyrate.

Table 1: Short-chain fatty acid content (g/L) of 12 and 24 h human faecal fermentations.

	FOS		**Raftilose**		**no Carbon**	
	12h	24h	12h	24h	12h	24h
Formate	1.43	1.42	2.11	1.49	1.14	0.96
Acetate	1.84	2.29	2.90	3.00	1.77	3.68
Propionate	2.35	2.41	3.49	2.29	0.36	1.40
iso-Butyrate	2.21	2.48	3.62	1.92	2.80	2.23
n-Butyrate	0.28	0.10	0.27	0.06	0.52	1.02

Given the low volumes obtained from both fermentation batches, the 24 h fermentation products were used for the proliferation studies with Caco-2 cells and the 12 h fermentation products were used for all studies with the Caco-2/HT29-MTX co-cultures.

II.2. Intestinal epithelium model based on Caco-2 cells

The products obtained from the *in vitro* human faecal fermentations were first tested in a simple intestinal epithelium model based on a Caco-2 cell monolayer to optimise both sample concentration and incubation time. Samples fermented with no carbon source and the fermentation media (FM) used in the *in vitro* human faecal fermentations were tested as controls.

The metabolic activity of Caco-2 cells after incubation with the *in vitro* human faecal 24 h-fermentation products was assessed by the resazurin reduction assay. The samples were diluted in culture media at different volume ratios (1:10, 1:6 and 1:3) and added for incubation with cells for 24 or 48 h. The sample dilutions led to a decrease in the pH of the cell culture media, which was dependent on the dilution ratio, being more significative for the samples fermented with both carbon sources (Table 2).

Figure 12 shows that after 24 h of incubation, all samples showed no significant effects on the cell metabolic activity at the 1:10 and 1:6 dilutions. However, at the highest concentration (1:3 dilution), the fermentation products with raftilose and FOS-enriched media showed a significant decrease ($p<0.05$) in the metabolic activity of Caco-2 cells (< 80%).

After 48 h of incubation, there was a general reduction of the cell metabolic activity, which was significant ($p<0.01$) for all samples at the 1:3 dilution, for the samples grown in raftilose and in the absence of a carbon source at the 1:10 and 1:6 dilutions and also in the fermentation media at 1:6 dilution.

Table 2: pH values of samples (products of *in vitro* human faecal fermentation, using different carbon sources) diluted in MEM at different ratios (1:10, 1:6 and 1:3). Values show Mean ± SD (N=3).

	Sample ratio			MEM
	1:10	1:6	1:3	
Fermentation media (FM)	7.48 ± 0.13	7.29 ± 0.05	7.22 ± 0.07	7.49 ± 0.12
No Carbon (nC)	7.49 ± 0.11	7.34 ± 0.14	7.30 ± 0.06	
Raftilose (R)	6.92 ± 0.46	6.99 ± 0.09	6.72 ± 0.11	
FOS (F)	7.10 ± 0.08	7.08 ± 0.12	6.65 ± 0.10	

The highest reduction was observed after 48 h of incubation, in cells incubated with the fermentation products from media supplemented with raftilose and FOS diluted 1:3, which led to metabolic activities lower than 50%.

These results suggest that the effect of the tested fermentation products on the metabolic activity of Caco-2 cells is dependent on both concentration and incubation time. The lower metabolic activity of cells incubated with FOS and Raftilose fermentation products at the higher concentrations (ratio 1:3) can also be associated with the significant decrease in pH. The fermentation products of human faecal samples were not toxic to Caco-2 cells at the 1:10 and 1:6 dilutions at the 24 h time point. Thus, the dilution ratio used in the following experiments was 1:6, as this concentration did not compromise cell viability after 24 h and still provides a significant concentration of fermentation products.

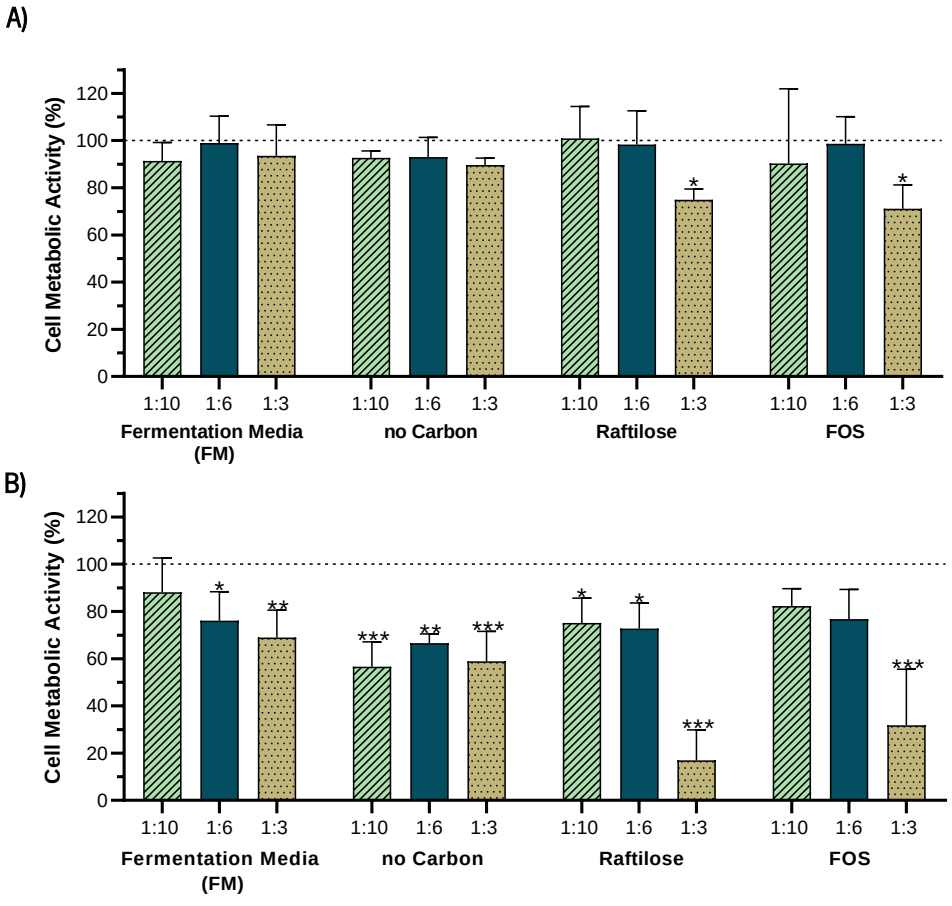

Figure 12: Effect of human faecal fermentation products, obtained in different fermentation media, on the proliferation of semi-confluent Caco-2 cells. Cell metabolic activity of Caco-2 cells incubated for (A) 24 or (B) 48h in MEM supplemented (1:10; 1:6 or 1:3) with fermentation media (FM) or products of fermentation of human faecal samples with no carbon source (no Carbon), raftilose (Raftilose) or fructo-oligosaccharides (FOS). The cell metabolic activity was determined by measuring the fluorescence of resofurin (λ_{ex}= 560 nm, λe_m= 590 nm) from the resazurin reduction assay. Values show Mean ± SD (N≥3; *p < 0.05; **p < 0.01; ***p < 0.001 *vs* control (untreated cells – dotted line at 100%) with p-values obtained using a two-way analysis of variance (ANOVA) with Tukey's post-hoc test for samples that followed a normal distribution according to the Shapiro-Wilk test).

CHAPTER III. Effect of ECM coatings and pore size on Caco-2/HT29-MTX co-cultures grown on transwell membranes

As described in Chapter I of this thesis, mono or co-cultures of epithelial cells on semi-permeable membranes are frequently used for *in vitro* studies of intestinal barrier integrity, bioactive compound uptake/permeability, and general toxicological studies. In addition, semi-permeable membranes are also often integrated as part of dynamic digestion models or advanced organ-on-chip devices[57].

The membrane pore size is a critical parameter, which plays a direct role on cell transmigration and biochemical communication. Typically, membranes with smaller pore sizes (0.4 or 1 μm) are used for permeability studies as these offer enough support for culturing cells and are large enough to allow the permeation of small molecules, nanoparticles and even small microparticles. Larger pore sizes (3 and 8 μm) are typically used for studies involving cell migration and are often included in some dynamic cell-culture models as is the case of the Gut-on-a-chip model developed at the Wyss Institute, which uses Caco-2 cells on a microfabricated 8-μm pore size membrane[81,82]. However, up to the best of our knowledge, there are no studies comparing the phenotype of co-cultures of Caco-2 and HT29-MTX on small and large pore-size membranes.

Cell adhesion, proliferation, phenotype and function may be influenced by the addition of functional coatings using ECM proteins[82,83]. The ECM provides the essential physical scaffold for cell adhesion[84]. Most cells need to attach (anchorage-dependent) to the ECM to survive and proliferate. The cellular response to the ECM is variable and different ECM proteins are used in tissue culture to modify cell behaviour[83]. Collagen is the most abundant fibrous protein within the ECM and provides tensile strength, regulates cell adhesion and directs tissue development[84]. Matrigel, a gelatinous protein mixture derived from mouse tumour cells, is commonly used as a membrane matrix[85].

To understand how different coatings and pore sizes influence the growth of Caco-2 and HT29-MTX cells in co-culture, Millicell® 12-well hanging inserts with 1 or 8 μm pore sizes were used uncoated, or coated with collagen (COL) or a mixture of collagen and Matrigel (COL + MAT). The cells were grown for 21 days and the TEER was monitored to assess the barrier integrity throughout the differentiation process. The permeability of propranolol [from the apical to basolateral side (A-B)], as a model compound of high permeability (transcellular transport), was assessed on differentiated monolayers to compare different experimental conditions (coatings and pore sizes)[86].

III.1. ECM coatings

Collagen (50 µg·mL^{-1}) and a mixture of collagen and Matrigel (50 µg·mL^{-1} and 300 µg·mL^{-1}, respectively) were tested as coatings of a commercial membrane with different pore sizes (1 or 8 µm).

The TEER measurement can be useful to conclude about cytotoxicity of samples in epithelial cell layers or any effect on barrier integrity. Cell culture models have been established to study epithelial transport in which TEER measurements provided useful information. The damage of the barrier integrity will be reflected on the reduction of the TEER or inversely, a tighter monolayer will present superior values of TEER[87].

Figure 13 shows the TEER of Caco-2/HT29-MTX co-cultures grown on 1 µm (A) or 8 µm (B) pore size membranes (uncoated, COL, COL+MAT), for 21 days. The TEER values of uncoated inserts were in keeping with previous publications using co-cultures of Caco-2/HT29-MTX[88,89]. During the course of the experiment there were no significant differences between the 3 coating conditions tested - uncoated inserts, and inserts coated with either collagen or a collagen/Matrigel mixture.

Although some differences in the TEER of coated inserts reached statistical significance (owing to low standard deviations), these were equal or lower than a 0.2-fold difference from the uncoated control (1965 Ω.cm^2 for collagen-coated inserts vs 1591 Ω.cm^2 for uncoated inserts at day 21).

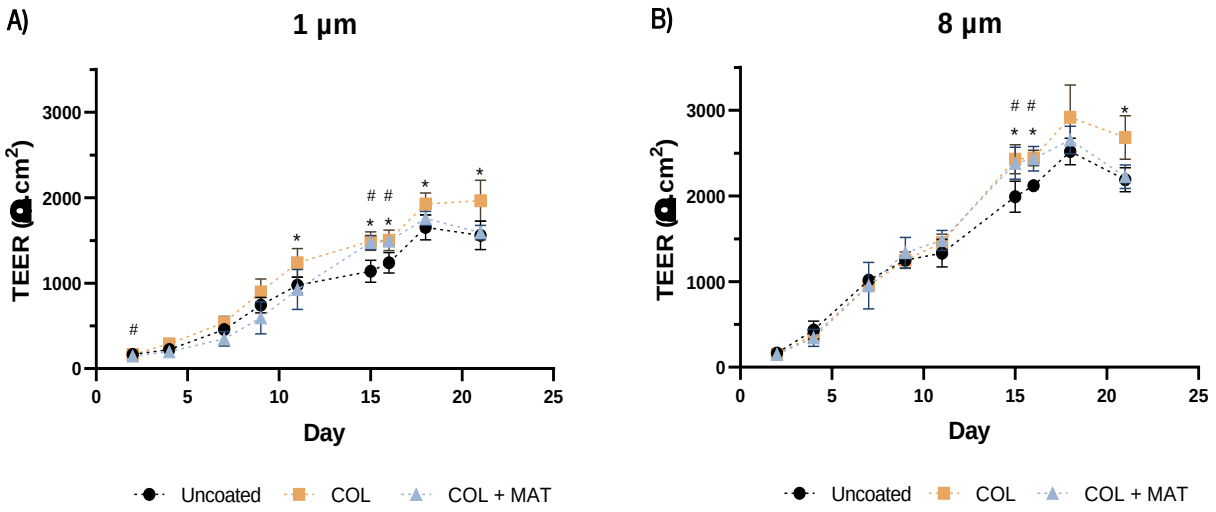

Figure 13: **Trans-epithelial electrical resistance (TEER) of Caco-2/HT29-MTX co-cultures grown for 21 days** on the apical side of (A) 1 µm or (B) 8 µm pore size Millicell® hanging inserts used uncoated, or coated with collagen (COL) or a mixture of collagen and Matrigel (COL + MAT). Values show Mean ± SD (N≥3; $^{*,\#}p < 0.05$ vs control (uncoated) with p-values obtained using the Student's t-test for independent samples that followed a normal distribution according to the Shapiro-Wilk test. *p: COL and $^{\#}p$: COL + MAT.)

These results were supported by the intestinal permeability assay, which showed no significant differences ($p>0.05$) in the apparent permeability of propranolol, over time, between the 3 coating conditions tested (**figure 14**). This could be anticipated given the TEER correlates directly with cohesion of the tight junction complexes. Thus, barriers with similar TEER should show similar intestinal permeability[90].

Propranolol is reported to have a human absorption >90% exhibiting high permeability values in both Caco-2 and Caco-2/HT29-MTX monolayers (P_{app} (A-B) > 1.0 x 10^{-5} cm.s^{-1})[86,91].

Overall, the results from the TEER monitoring over the cellular differentiation process and the *in vitro* intestinal permeability assay suggest that the coatings tested do not have a considerable effect on the epithelial barrier integrity and transcellular transport of propranolol across the Caco-2/HT29-MTX monolayer.

Given that there were no significant differences between the coating conditions tested. For simplicity, the following experiments were conducted using uncoated inserts.

III.2. Pore size

The effect of the pore size (1 µm or 8 µm) on the differentiation process of Caco-2/HT29-MTX co-cultures was evaluated through TEER, confocal microscopy and by assessing propranolol permeability.

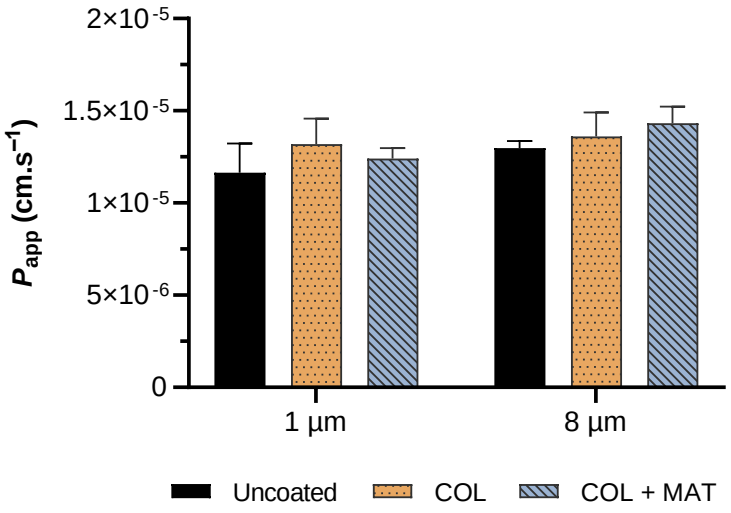

Figure 14: **Apparent permeability of propranolol across a Caco-2/HT29-MTX co-culture** from the apical to the basolateral chamber of a transwell™ system. Cells were grown on (A) 1 µm or (B) 8 µm pore size Millicell® hanging inserts coated with collagen (COL) or a collagen and Matrigel mixture (COL + MAT). Uncoated Millicell® inserts were used as controls. Values show Mean ± SD (N≥3).

Figure 15 shows that the TEER of Caco-2/HT29-MTX co-cultures was significantly higher for cells cultured on the 8 µm pore size inserts when compared to 1 µm pore size ($p<0.05$). This tendency was observed independently of the coating condition tested (**figure 15 A-C**).

In the literature is reported that cell migration can occur through pores larger than 3 µm[92]. **Figure 16** shows that a fraction of the cells seeded on the 8 µm pore-size inserts migrated to the basolateral side of the chamber forming an additional epithelial barrier, and thus potentially leading to higher TEER values. This double layer in the basolateral side of the membrane was not observed for the 1 µm pore-size inserts.

These results are in line with previous studies that suggest that the discontinuous nature of porous membranes and the small pore spacing affect cell-substrate interactions. Limited contact regions weaken cell-surface interactions promoting instead cell-cell interactions[93].

The TEER was further monitored throughout the intestinal permeability assay. **Figure 17** shows that the TEER of the 8 µm inserts dropped significantly between the end of the differentiation process (before) and the starting point of the permeability assay (0 h) (>2000 $\Omega.cm^2$ and <1000 $\Omega.cm^2$, respectively). It should be pointed out that there are some manipulations in between, such as the removal of the culture medium, washes with HBSS and the addition of new HBSS for the permeability study. Additionally, during and after the assay, the TEER was significantly lower ($p<0.05$) for cells grown on the 8 µm pore size membranes than on the 1 µm pore size membranes. In turn, the TEER values obtained for the 1 µm inserts remained fairly constant throughout the whole experiment (1000 $\Omega.cm^2$<TEER<1500 $\Omega.cm^2$).

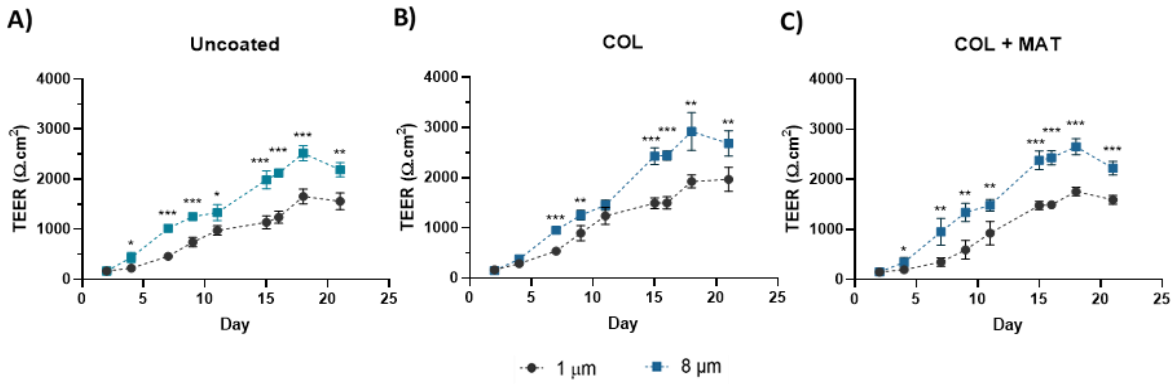

Figure 15: Trans-epithelial electrical resistance (TEER) of Caco-2/HT29-MTX co-cultures grown for 21 days on the apical side of 1 µm and 8 µm pore size Millicell® hanging inserts used (A) uncoated and coated with (B) collagen (COL) or (C) a mixture of collagen and Matrigel (COL + MAT). Millicell® inserts without coatings (Uncoated) were used as controls. Values show Mean ± SD (N≥3; *$p < 0.05$; **$p < 0.01$; ***$p < 0.001$ vs control (Uncoated) with p-values obtained using the Student's t-test for independent samples that followed a normal distribution according to the Shapiro-Wilk test).

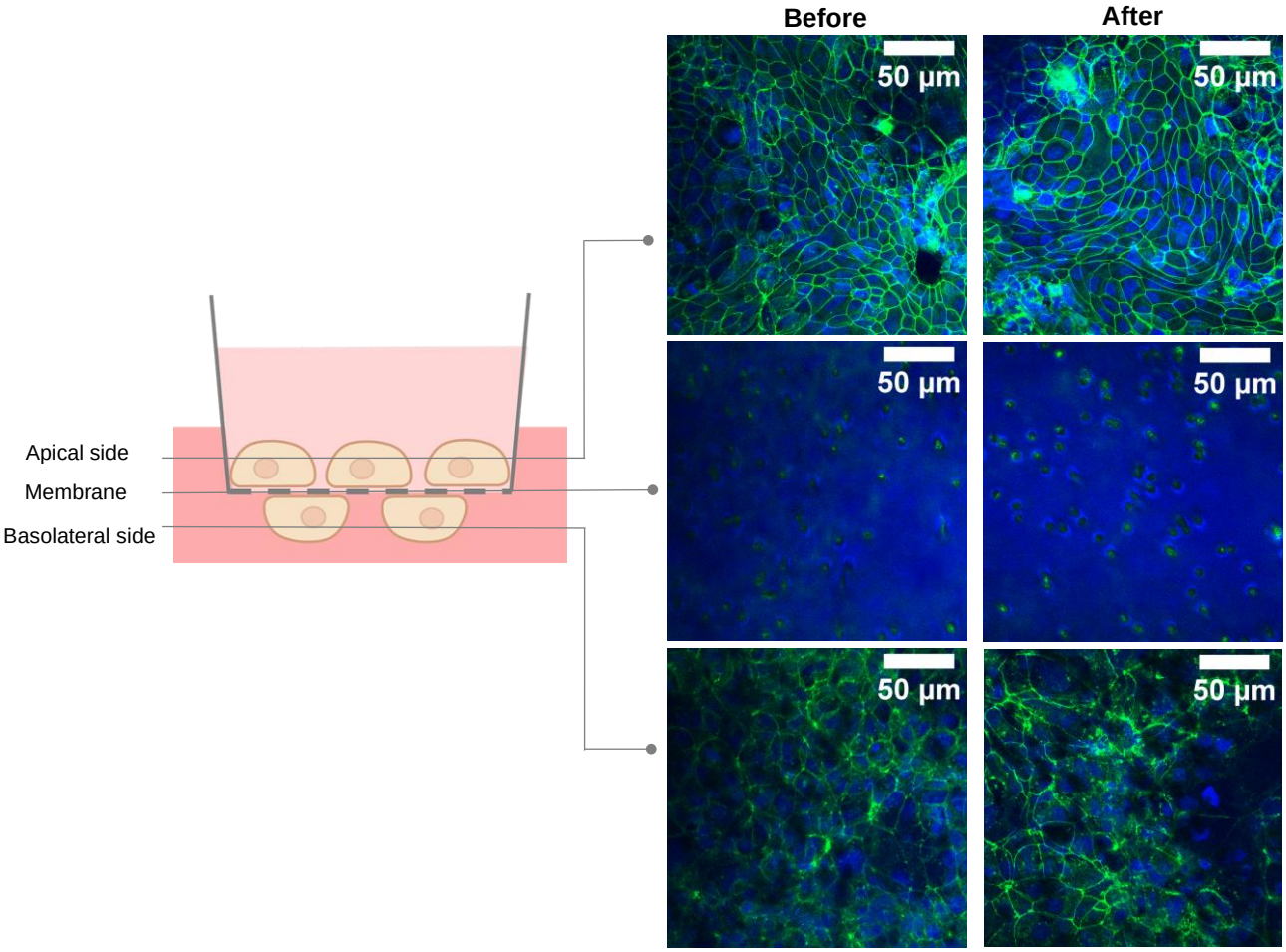

Figure 16: **Confocal microscopy images** of Caco-2/HT29-MTX co-cultures stained for occludin (green) and nuclei (DAPI, blue) of Caco-2/HT29-MTX co-cultures grown on **8 µm pore size Millicell® hanging inserts used uncoated**. Images were taken **before and after the permeability assay**.

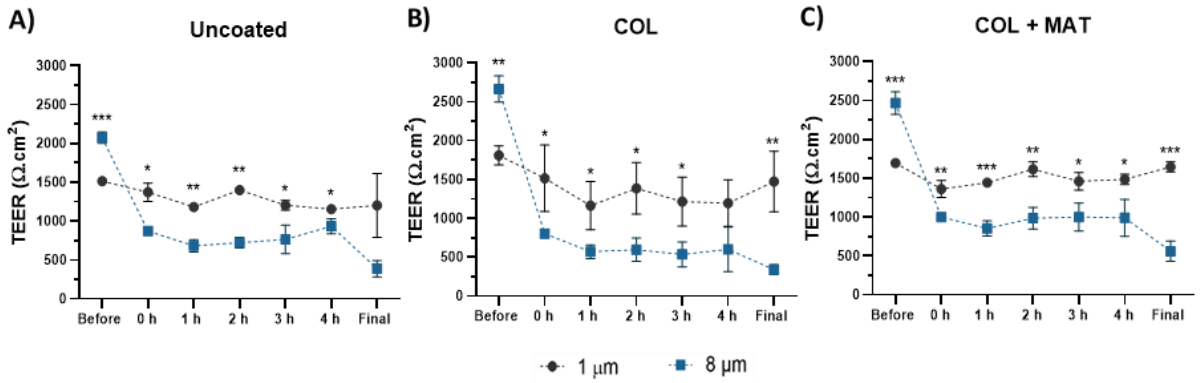

Figure 17: **Trans-epithelial electrical resistance (TEER) of Caco-2/HT29-MTX co-cultures during the intestinal permeability assay**. During 4 h, TEER was measured on 1 µm and 8 µm pore size Millicell® hanging inserts used (A) uncoated and coated with (B) collagen (COL) or (C) a mixture of collagen and matrigel (COL + MAT). Millicell® inserts without coatings (Uncoated) were used as controls. Values show Mean ± SD (N≥2; *p < 0.05; **p < 0.01; ***p < 0.001 with p-values obtained using the Student's t-test for independent samples that followed a normal distribution according to the Shapiro-Wilk test).

Although not quantitative, **Figure 18** shows that there were no visible differences between the expression of the tight junction-specific protein occludin in the 1 µm and 8 µm pore size conditions. Tight junctions seem to have been maintained along the permeability assay, for both pore sizes membranes, in the monolayer at the apical side of the membrane. This way, the decrease of the TEER seems not to be associated with a decrease in tight junctions of the cellular monolayer obtained in the apical side of the 8 µm membranes. However, small damages could not be observable or some cells in the basolateral side of the membrane can be more susceptible to manipulations and be easily removed during the cells´ washes before the permeability study, leading to the TEER decrease. In addition, cells appear to be more densely packed on the 1 µm membranes. Despite the constant values of permeability obtained, the cumulative fraction of propranolol transported is indeed higher in 8 µm pore size membranes (**figure 19**).

In addition, the difference on the pore density of the 1 µm and 8 µm membranes (technical information from supplier, $2x10^6/cm^2$ vs $2x10^5/cm^2$) leads to the total area occupied by pores in the 8 µm membrane to exceed that of the 1 µm membrane by nearly 6-fold (0.11 cm^2 vs 0.02 cm^2). In other words, on 1 µm inserts approximately 98% of the total surface area is available to support cells allowing the establishment of focal adhesions whereas, on 8 µm membranes this is reduced to just 90%. Altogether, this can lead to the conclusion that cells on 8 µm membranes are likely to be more susceptible to manipulation during experiments, and thus vulnerable to the creation of small defects in the epithelial monolayer.

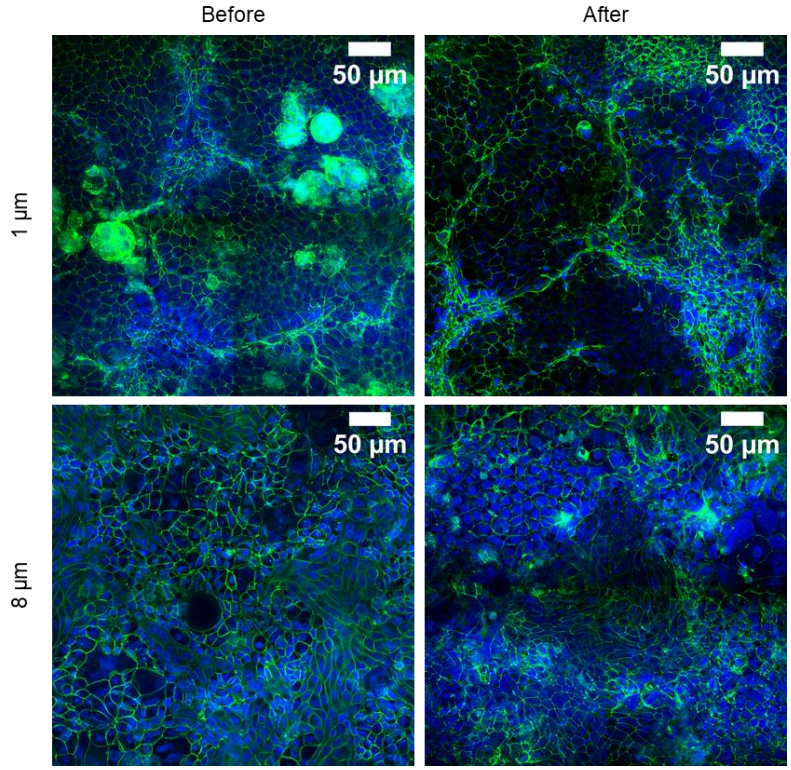

Figure 18: **Confocal microscopy images** of occludin (green) and nuclei (DAPI, blue) of Caco-2/HT29-MTX co-cultures grown on **1** and **8 µm pore size Millicell® hanging inserts used uncoated**. Images were taken **before and after the permeability assay**.

These results reiterated that pore size and density of cell culture membranes play an important role on the intestinal epithelial barrier integrity, on the morphology of the cell layer and on transcellular permeability. Since 1 µm membranes showed more consistent results these were used on the following studies of this work.

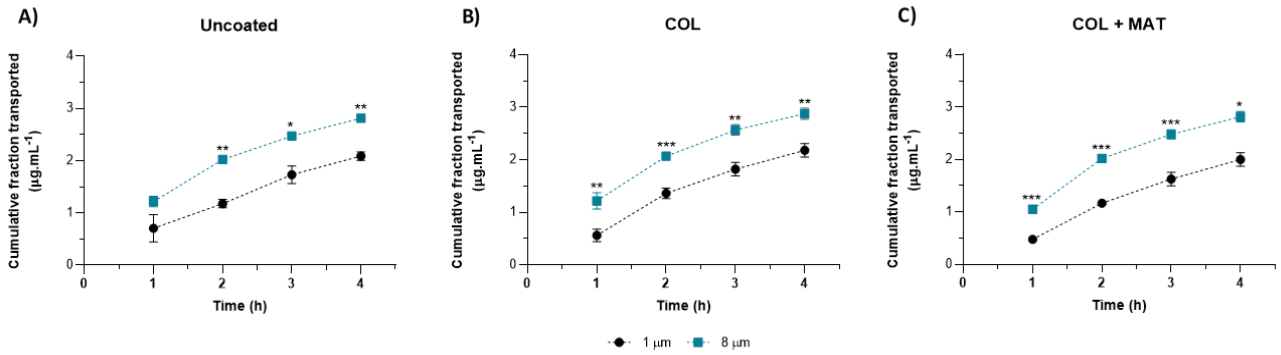

Figure 19: **Cumulative fraction of propranolol transported across a Caco-2/HT29-MTX co-culture** from the apical to the basolateral chamber of a transwell™ system. Cells were grown on 1 µm and 8 µm pore size Millicell® hanging inserts used (A) uncoated and coated with B) collagen (COL) or a (C) collagen and matrigel mix (COL + MAT). Millicell® inserts without coatings (Uncoated) were used as controls. Values show Mean ± SD (N≥2; *p < 0.05; **p < 0.01; ***p < 0.001 with p-values obtained using the Student's t-test for independent samples that followed a normal distribution according to the Shapiro-Wilk test).

CHAPTER IV. Effect of *in vitro* human faecal fermentation products on the proliferation of Caco-2/HT29-MTX co-culture

Caco-2/HT29-MTX co-cultures were used as a more complex intestinal epithelium model. To understand the effect of *in vitro* human faecal fermentation products in the intestinal epithelium, the Caco-2/HT29-MTX co-culture was used to study cell viability, production of reactive oxygen species, inflammatory response, intestinal permeability, transepithelial electrical resistance and expression of tight-junction specific proteins.

The metabolic activity of the Caco-2/HT29-MTX co-cultures after incubation with the human faecal fermentation products (diluted 1:6 in cell culture media) for 24 h was assessed by the resazurin assay. **Figure 20** shows that after 24 h of incubation, there were no significant differences ($p>0.05$) between all samples tested and the control (cells grown in MEM) leading to the conclusion that the human faecal fermentation products appear to be non-toxic towards the Caco-2/HT29-MTX co-cultures.

The TEER values of Caco-2/HT29-MTX co-cultures throughout the 21 days of differentiation, on the uncoated 1 µm pore size Millicell® membranes (**appendix G**) were in keeping with the results obtained previously for uncoated 1 µm membranes (**figure 13**).

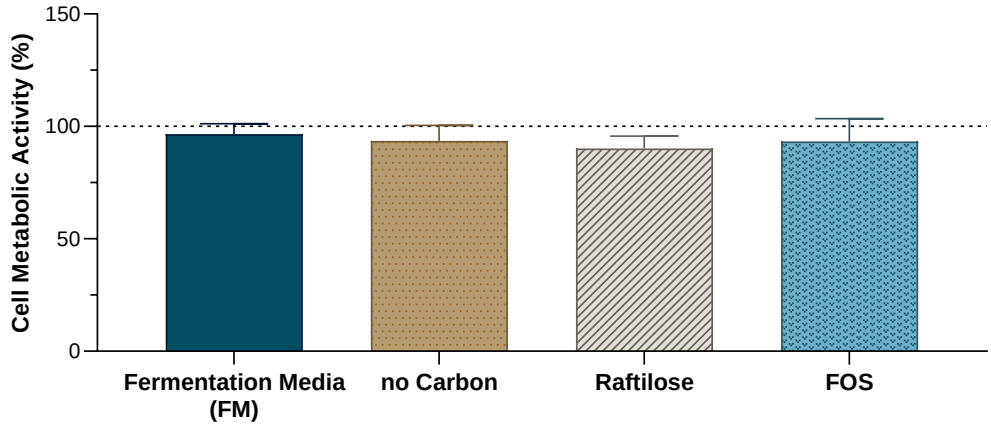

Figure 20: **Effect of human faecal fermentation products, obtained in different fermentation media, on the proliferation of Caco-2/HT29-MTX co-cultures.** Metabolic activity of Caco-2/HT29-MTX co-cultures incubated for 24h in MEM supplemented (1:6) with fermentation media (FM) or products of fermentation of human faecal samples with no carbon source (no Carbon) or supplemented with raftilose (Raftilose) or fructo-oligosaccharides (FOS). The cell metabolic activity was determined by measuring the fluorescence of resofurin (λex= 560 nm, λem= 590 nm) from the resazurin reduction assay. Values show Mean ± SD (N=12 from 3 independent assays). A two-way analysis of variance (ANOVA) with Tukey's post-hoc test for samples that followed a normal distribution according to the Shapiro-Wilk test) was conducted. Test conditions *vs* control (MEM - dotted line at 100%) show no significant differences.

In a previous report, fermentation products from prebiotic fibres have been shown to significantly increase the TEER of Caco-2/HT29-MTX co-cultures and therefore have an increase in the integrity of the intestinal barrier[94]. In this work, after differentiation (21 days in culture), the co-cultures were incubated with propranolol (100 µM) in the presence of human faecal fermentation products (diluted 1:6) for 4 hours, during which the TEER remained unchanged (**figure 21**).

These differences can be explained by the period of differentiation of the cells in co-culture. In the mentioned report, cells were used during the differentiation process (13 days) whereas, in this work cells were used only after it (21 days). It is possible that during the differentiation process, cells are more susceptible to external factors which could lead to a more pronounced effect by the fermentation products.

Figure 22 shows a significant decrease ($p<0.01$) in the apparent permeability of propranolol obtained for cells incubated with faecal fermentation products when compared to cells in HBSS (control).

The decrease in apparent permeability and accompanying reduced transport of propranolol (**appendix H**), typically reflect a tighter intestinal epithelial barrier. However, given the TEER was unchanged, any paracellular transport should not have been significantly affected.

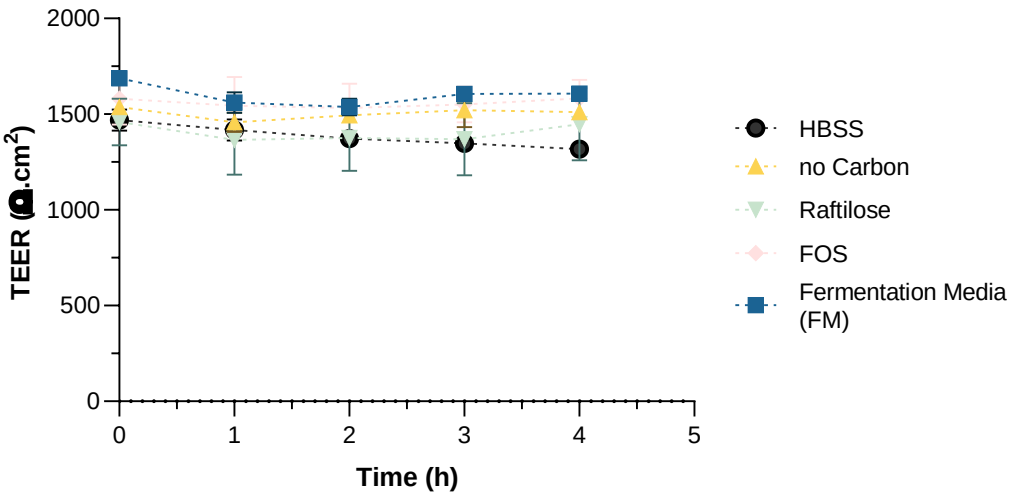

Figure 21: Trans-epithelial electrical resistance (TEER) of Caco-2/HT29-MTX co-cultures exposed to fermentation media (FM) or products of human faecal fermentation during the intestinal permeability assay. During 4 h, TEER was measured on 1 µm Millicell® hanging inserts used uncoated. Values show Mean ± SD (N=4; from 1 independent assay). A two-way analysis of variance (ANOVA) with Tukey's post-hoc test for samples that followed a normal distribution according to the Shapiro-Wilk test) was conducted. Test conditions vs control (MEM - dotted line at 100%) show no significant differences.

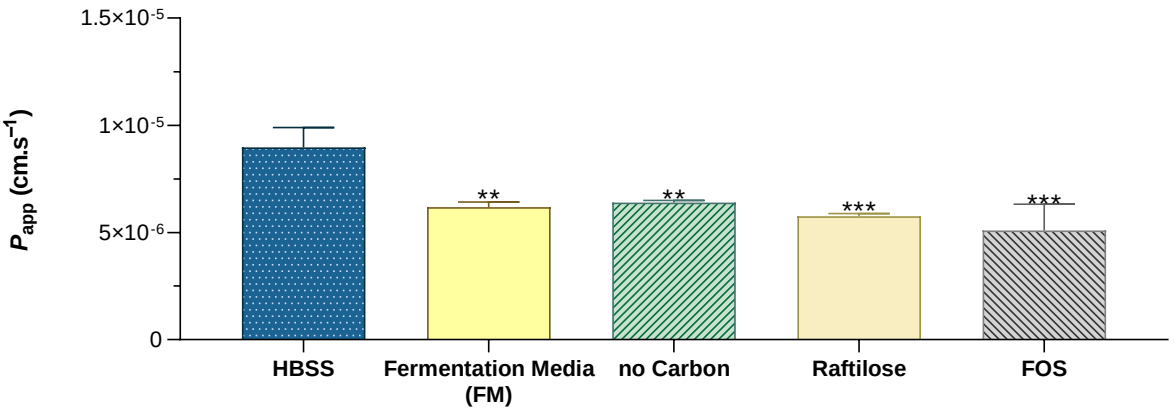

Figure 22: Apparent permeability of propranolol across a Caco-2/HT29-MTX co-culture exposed to human faecal fermentation products from the apical to the basolateral chamber of a cell culture insert. Propranolol and fermentation media (FM) or products of fermentation of human faecal samples in media with no carbon source (no Carbon), or with raftilose (Raftilose) or fructo-oligosaccharides (FOS), diluted in HBSS-HEPES (dilution 1:6), were incubated for 4h. Values show Mean ± SD (N≥3; **p < 0.01; ***p < 0.001 vs control (HBSS) with p-values obtained using a two-way analysis of variance (ANOVA) with Tukey's post-hoc test for samples that followed a normal distribution according to the Shapiro-Wilk test).

Propranolol, as a beta-adrenergic receptor blocker is member of the large family of G protein-coupled receptors (GPCRs)[95,96]. In turn, SCFA present in the faecal fermentation products may activate signalling pathways via at least 3 different GPCRs (GPR41, GPR43 and GPR109A)[26]. Thus, these results could reflect competitive binding between the SCFA and propranolol to the same receptors for transcellular transport. Moreover, the constant TEER throughout the permeability assay indicates that the integrity of the intestinal barrier is not compromised by the human faecal fermentation products, in the tested concentrations.

The integrity of the intestinal epithelial barrier after the permeability assay was further verified by the confocal images shown in **figure 23.**

Cells grown in the presence of the faecal fermentation products showed a consistent expression of the tight junction-specific protein occludin and displayed a similar morphology to cells grown in control conditions (HBSS).

Future work could include the individual analysis of SCFA (formate, acetate, propionate and butyrate) to understand if there is a competitive binding of each SCFA and propranolol to the same receptors.

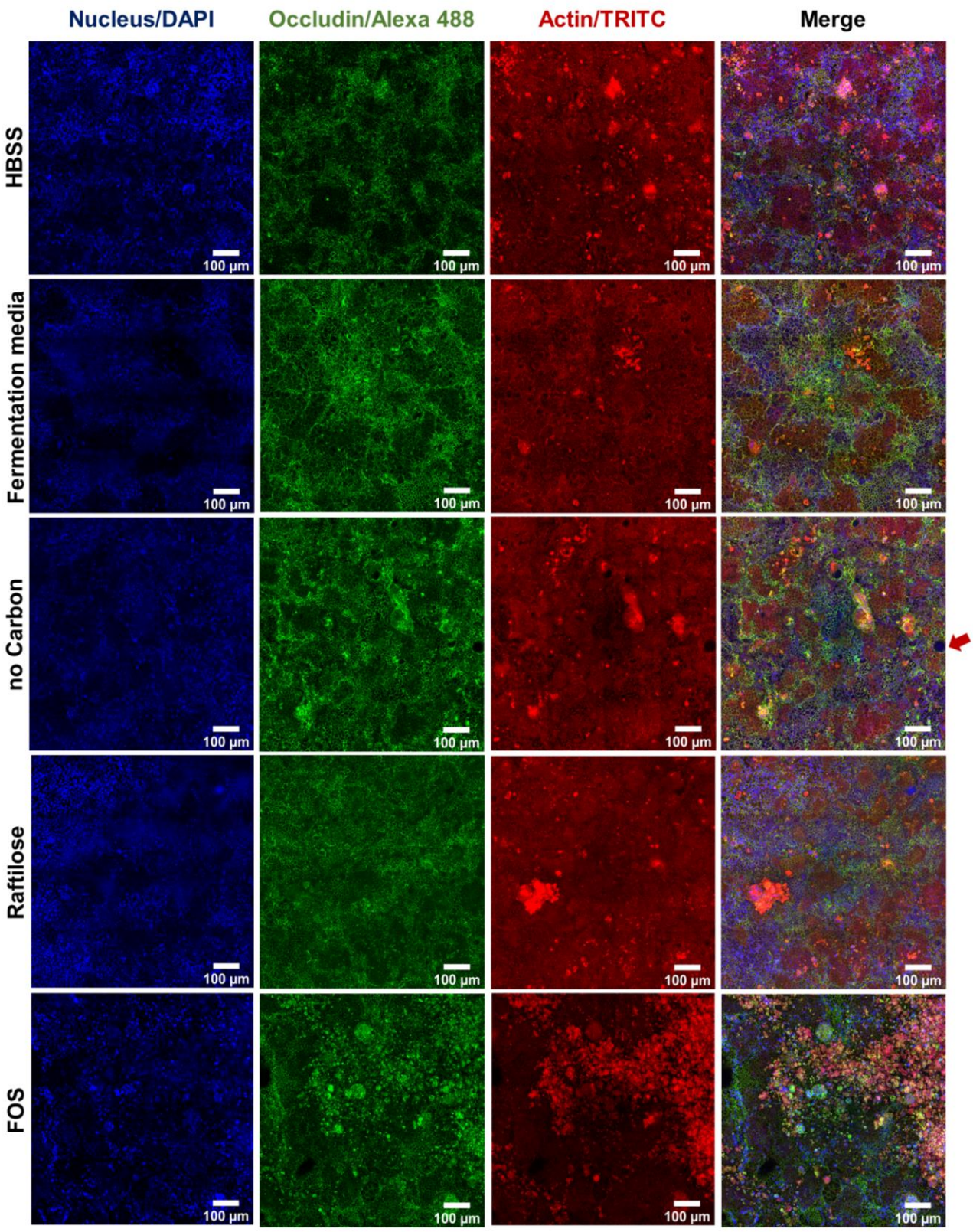

Figure 23: **Tile scan confocal microscopy images** 40x magnification of of Caco-2/HT29-MTX co-cultures grown on **1 pore size Millicell® hanging inserts**, stained for occludin (green), actin (red) and nuclei (DAPI, blue)**.** Images were taken **after the permeability assay**. Propranolol and fermentation media (FM) or products of fermentation of human faecal samples in media with no carbon source (no Carbon), or with raftilose (Raftilose) or fructo-oligosaccharides (FOS), diluted in HBSS-HEPES (dilution 1:6), were incubated for 4h.

The confocal microscopy images in **figure 23** show some areas which, at first site, are cell-free (red arrow shows an example in the 'no Carbon' condition). However, closer investigation by images taken at higher resolution and in different confocal planes showed that these are actually domes, as shown by the orthogonal cross-sectional views in **figure 24**.

The formation of domes is an example of bending morphogenesis[97]. Domes are considered a specialized cell organization in charge of transepithelial transport properties which are a good indication of epithelial differentiation[98]. The factors that drive dome's formation are not fully understood. *In vitro* domes are thought to be formed by the following steps: 1) Transcellular transport of ions increases the interstitial concentration of ions at the basal side, 2) The osmotic gradient is increased by the ion transport resulting on fluid influx to the basal side and 3) Hydrostatic pressure is generated by the formation of fluid-induced domes. These structures are observed both *in vivo* and *in vitro* but there are notable differences between them. *In vitro* domes repeat the process of collapse and formation while *in vivo* domes in vilification maintain their shape. The stability differences probably result from the different scaffolds. The basal side of *in vitro* domes are filled with fluid while the basal side of *in vivo* domes, the *lamina propria*, is rich in ECMs, which provides 3D structural support[97].

Figure 24 A shows in detail a dome which is likely filled with fluid. In **figure 24 B** it can be seen that the top of the dome is completely closed, and the membrane is indeed covered with cells.

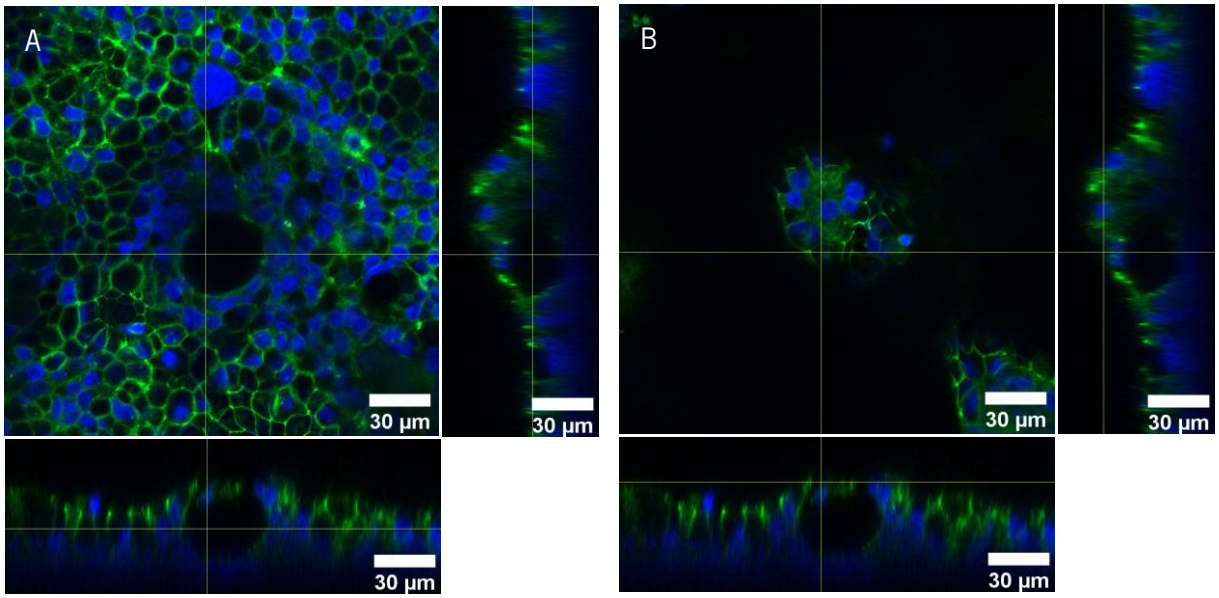

Figure 24: **Confocal microscopy images of Caco-2/HT29-MTX co-cultures** grown on uncoated 1 pore size Millicell® hanging inserts stained for occludin (green) and nuclei (DAPI, blue). **Images were taken after the permeability assay.** Propranolol and fermentation media (FM) or products of fermentation of human faecal samples in media with no carbon source (no Carbon), or with raftilose (Raftilose) or fructo-oligosaccharides (FOS), diluted in HBSS-HEPES (dilution 1:6), were incubated for 4h. **A) Area with a dome, B) Top of the columnar formation.**

The generation of intracellular ROS was evaluated by using oxidation sensitive DCFH-DA. The oxidative activity of human faecal 12h-fermentation products was tested. Caco-2/HT29-MTX co-cultures were incubated with DCFH-DA for 1h, after which the solution was removed, and replenished by test samples diluted in HBSS (ratio 1:6). H_2O_2 was used as a positive control. **Figure 25 (A)** shows that the intracellular ROS production of cells incubated for 4 h with the faecal fermentation products from raftilose or FOS enriched media were unchanged when compared with the control (cells grown in HBSS). However, the fermentation media (FM) showed a significant increase ($p<0.001$) in the intracellular production of ROS, which was even higher than for H_2O_2 (positive control). The fermentation media (FM) is very complex, containing multiple ingredients such as trypticase soy broth, bactopeptone and yeast nitrogen base that are intended for bacterial cell culture. These ingredients as they are not metabolised by the microbiota, may induce the formation of ROS, thus potentially explaining the effect observed here.

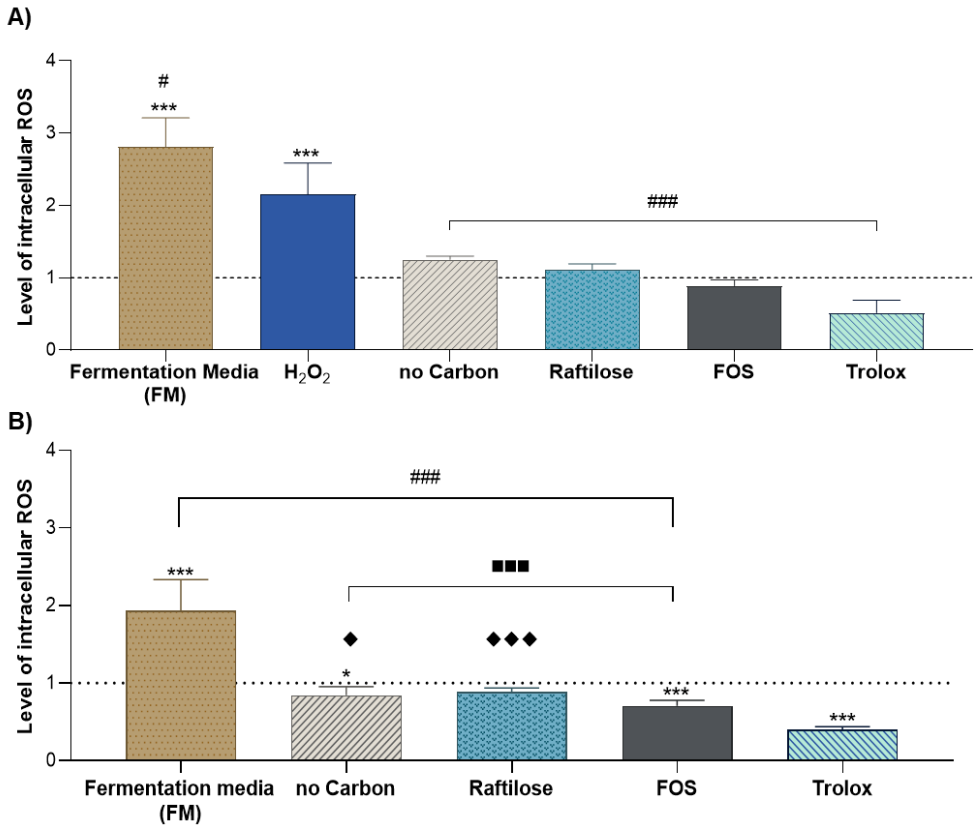

Figure 25 (A) Intracellular production of ROS by Caco-2/HT29-MTX co-cultures exposed to HBSS (control), 50 µg.mL-1 Trolox (negative control), 2.5 mM H_2O_2 (positive control), fermentation media (FM), products of fermentation of human faecal samples in media with no carbon source (no Carbon), with raftilose (Raftilose) or fructo-oligosaccharides (FOS), diluted in HBSS-HEPES (dilution 1:6), for 4h. **(B) Caco-2/HT29-MTX co-cultures further stressed with 2.5 mM of H_2O_2**. The production of ROS was determined by measuring the fluorescence of DCF (λex= 495 nm, λem= 525 nm) from the DCFH-DA reduction assay. Values show Mean ± SD (**(A)** N=16 from 4 independent assays; ***$p < 0.001$ vs control (HBSS - dotted line at 1); $^{\#}p<0.05$ vs H_2O_2 p-values (B) N=12 from 3 independent assays; *$p < 0.05$; ***$p < 0.001$ vs control (HBSS - dotted line at 1); ###$p<0.001$ vs Trolox; ■■■$p<0.001$ vs FM; ◆$p<0.05$, ◆◆◆$p<0.05$ vs FOS obtained using a two-way analysis of variance (ANOVA) with Tukey's post-hoc test for samples that followed a normal distribution according to the Shapiro-Wilk test).

The fermentation products of the 'no Carbon' condition also showed no increase in the production of ROS, likely owing to the occurrence of fermentation, further supporting the hypothesis suggested above.

In order to verify if the fermentation products of faecal samples have a protective effect against an oxidative stimulus, H_2O_2 (2.5 mM) was used as an oxidant agent. For this, following the 4 h incubation with the test samples, H_2O_2 was added for an additional hour. Trolox (50 $\mu g \cdot mL^{-1}$), a known antioxidant compound, was used as a negative control on the first 4 h incubation period.

Figure 25 (B) shows that cells incubated with the fermentation media (FM) show once again a significant ($p<0.001$) increase in the production of ROS. However, cells incubated with the faecal fermentation products of FOS show a significant ($p<0.001$) decrease on the production of ROS leading to the conclusion that FOS enriched media appears to be antioxidant.

SCFA are known for being mediators between the gut microbiota and the intestinal immune system. One of the regulation mechanisms is the regulation of leukocytes through the production of several cytokines and interleukins[99]. Systemic inflammation is mostly assessed by measuring TNF-α and INF-γ, and IL-1β, IL-6, IL-8 and IL-10[100]. IL-8 levels are low in a healthy intestinal epithelium but pro-inflammatory stimuli are known to increase its production[101]. TNF-α can stimulate the induction of various genes involved in inflammation including *CXCL8* responsible for the production IL-8[102].

With this in mind, the inflammatory response of cells incubated in the presence of the human faecal fermentation products was assessed by two different approaches: 1) detection of human IL-8 using the LEGEND MAX™ Human IL-8 ELISA Kit; and 2) quantification of the expression of inflammatory response mediators' genes - interleukin 1 beta (*IL1B*), interleukin 6 (*IL6*), C-X-C motif chemokine ligand 8 (*CXCL8*), tumor necrosis factor (*TNF*) and prostaglandin-endoperoxide synthase 2 (*PTGS2*) - by a two-step quantitative reverse transcription polymerase chain reaction (qRT-PCR).

Caco-2/HT29-MTX co-cultures were incubated with human faecal fermentation products diluted in MEM (ratio 1:6) for 4 h. Untreated cells and cells incubated with MEM supplemented with 50 $ng \cdot mL^{-1}$ of TNF-α were used as a negative and positive controls of inflammation respectively. After 4 h of incubation, the supernatant was collected and stored at -20 °C for later detection of IL-8 by the LEGEND MAX™ Human IL-8 ELISA Kit. The total RNA was extracted from the cells and a two-step qRT-PCR was performed.

Figure 26 shows the concentrations of human IL-8 (pg/mL) obtained from the supernatants of cells incubated with the test compounds. There was a 3-fold increase in the production of IL-8 when cells were stimulated with 50 ng·mL^{-1} TNF-α. On the other hand, cells incubated in the fermentation media or fermentation products from raftilose enriched media showed no effect on the cellular production of IL-8. The fermentation products from no carbon media and FOS enriched media induced a significant ($p<0.05$) decrease in the production of IL-8 when compared to the control condition (cells grown in MEM). However, though significant, the differences were minute (17 vs 12 pg/mL) and likely do not have biological significance. This was in keeping with the quantification of *CXCL8* expression by qRT-PCR (**figure 27**), which showed a 4-$\log_2$ increase by cells incubated with TNF-α, but no differences in all other conditions tested.

Likewise, the amplification of the *IL6* yielded high threshold cycle (C_t) values (>33, considered as not expressed) for all test conditions, except for the positive control ($31>C_t>33$). Interestingly, all test conditions (except the fermentation media) led to an increase in the expression of *TNF*. The expression profiles of the *IL1B* and *PTGS2* were similar showing a slight increase in expression in all conditions, except for the 'no Carbon' and the fermentation media condition. Note that the expression was at all times lower than that of the positive control (cells incubated with TNF- α).

Altogether, the IL-8 protein quantification and gene expression results indicate that the fermentation products tested here, at a 1:6 dilution, did not elicit a significant inflammatory response on the Caco-2/HT29-MTX co-culture model.

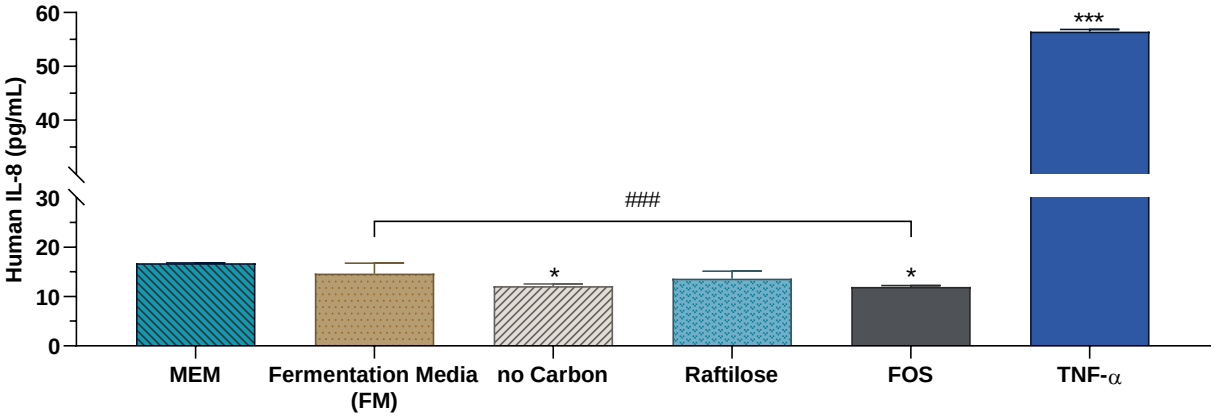

Figure 26: Production of human IL-8 (pg/mL) by Caco-2/HT29-MTX co-cultures exposed to MEM (negative control), 50 ng·mL^{-1} TNF-a (positive control), fermentation media (FM), products of fermentation of human faecal samples in media with no carbon source (no Carbon), with raftilose (Raftilose) or fructo-oligosaccharides (FOS), diluted in MEM (dilution 1:6), for 4h. Values show Mean ± SD (N=8 from 2 independent assays; *$p < 0.05$; ***$p < 0.001$ vs control (MEM); ###$p<0.001$ vs TNF- α p-values obtained using a one-way analysis of variance (ANOVA) with Tukey's post-hoc test for samples that followed a normal distribution according to the Shapiro-Wilk test).

Future work could include the analysis of potential anti-inflammatory action by assessing the expression of inflammatory response mediators' genes on a cellular model of inflammation, incubated with the faecal fermentation products.

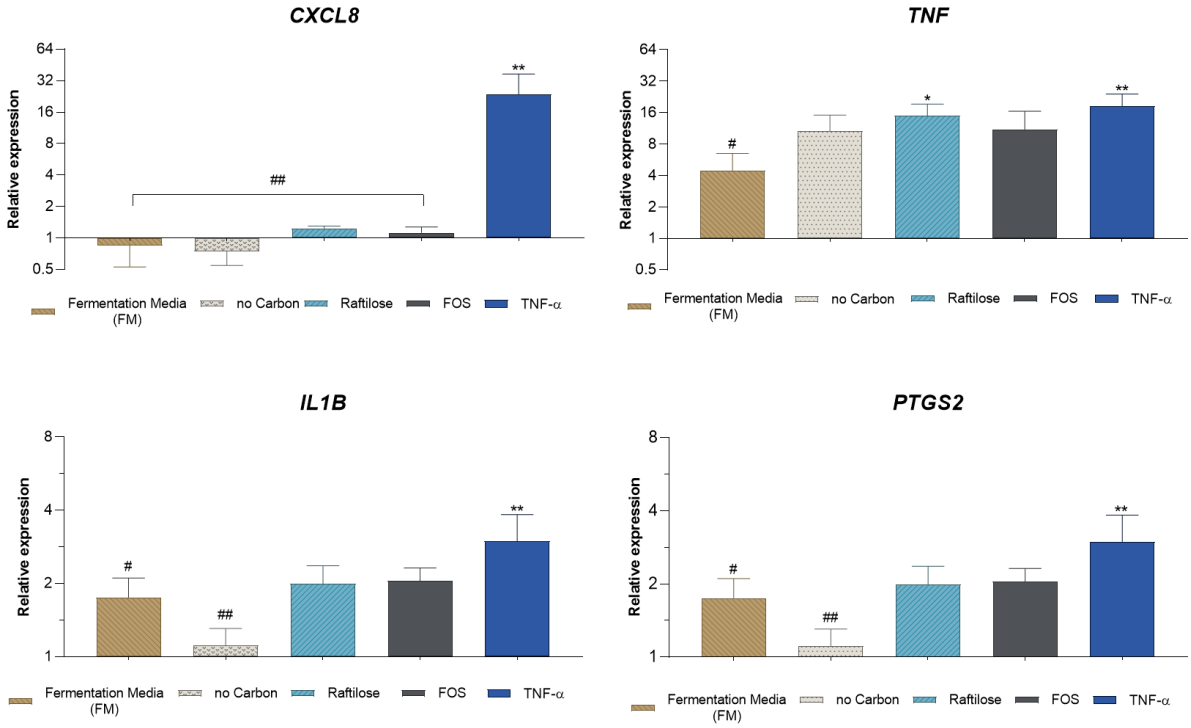

Figure 27: **Relative expression of *CXCL8*, *TNF*, *IL1B* and *PTGS2* by Caco-2/HT29-MTX co-cultures** exposed to MEM (negative control), 50 ng·mL^{-1} TNF-α (positive control), fermentation media (FM), products of fermentation of human faecal samples in media with no carbon source (no Carbon), with raftilose (Raftilose) or fructo-oligosaccharides (FOS), diluted in MEM (dilution 1:6), for 4h. Total RNA was extracted from the cells and reverse transcribed. The $2^{-\Delta\Delta Ct}$ method was used for relative quantification of gene expression, and the data were normalized to the expression of actin beta gene (*ACTB*) and compared to the expression levels of untreated cells. Values show Mean ± SD (N=3 from 3 independent assays; *p < 0.05; **p < 0.01 vs control (MEM); $^{\#}$p<0.05, $^{\#\#}$p<0.01 vs TNF- α p-values obtained using a one-way analysis of variance (ANOVA) with Tukey's post-hoc test for samples that followed a normal distribution according to the Shapiro-Wilk test).

Conclusions and future remarks

In the present work, the first tests concerning the development of the Colon-Host reactor were conducted. To optimize the cell-based module of the Colon-host reactor, a Caco-2/HT29-MTX cell culture model was used and the response of the intestinal *in vitro* epithelium to products of the fermentation of prebiotics by the human microbiota was studied.

Caco-2 cells experiments demonstrated that the effect of human faecal fermentation products on the metabolic activity is dependent on both concentration and incubation time. A dilution of 1:6 and a maximum incubation time of 24 h ensured the viability of Caco-2 cells and Caco-2/HT29-MTX cells grown in co-culture.

The integrity of the intestinal barrier was not compromised by the human faecal fermentation products from different fermentation media, since a constant TEER was observed throughout the permeability assay with propranolol. However, a significant decrease ($p<0.01$) in the apparent permeability of propranolol was observed for cells incubated with faecal fermentation products, when compared to cells in HBSS (control). A competitive binding between the SCFA and propranolol may had occurred. This way, future work could include the analysis of individual SCFA to evaluate if there is a competitive binding to the same receptors. In addition, any fermented sample induced oxidative stress in the Caco-2/HT29-MTX co-culture model. Moreover, fermentation products of FOS-enriched media significantly ($p<0.001$) decrease the intracellular ROS levels, leading to the conclusion that this fermentation product presents an antioxidant activity.

Regarding the inflammatory response, the fermentation products tested did not induced a significant inflammatory effect on the Caco-2/HT29-MTX co-culture model, according with the levels of IL-8 produced (ELISA quantification) and the inflammatory response mediators' genes expressed (qRT-PCR). Future work could include studies using a cellular inflammation model to evaluate the anti-inflammatory effect of fermentation products.

The response of the Caco-2/HT29-MTX co-culture model to the prebiotic fermentation products studied in this work provides a comparison to future works performed in the Colon-Host simulator. With these initial tests, protocols were established for a better representation of the intestinal *in vitro* epithelium and the cell-based module of the Colon-Host was optimized.

Materials and Methods

IV.1. Materials

Power SYBR® Green PCR Master Mix was obtained from **Applied Biosystems** (Foster City, CA, USA). Caco-2 cells were purchased from **American Type Culture Collection** (ATCC®). HT29-MTX-E12 cells were obtained from **European collection of Authenticated Cell cultures** (ECACC). Minimum essential media (MEM) Eagle was purchased from **PAN-Biotech GmbH** (Aidenbach, Germany). 96, 24 and 12-well plates were purchased from **TPP Techno Plastic Products AG** (Trasadingen, Switzerland). AllPrep DNA/RNA Mini Kit was purchased from **Qiagen** (Hilden, Germany). Acetonitrile was bought from **VWR** (Radnor, PA, USA). LEGEND MAX™ Human IL-8 ELISA Kit and tumour necrosis factor alpha (TNF-α) were bought from **BioLegend** (San Diego, CA, USA) .4′, 6-diamidino-2-phenylindole, dilactate (DAPI, Invitrogen™), Matrigel™ membrane matrix, rat tail type-I collagen and SuperScript™ VILO™ cDNA Synthesis Kit was purchased from **Thermo Fisher Scientific** (Waltham, MA, USA). Millex-GS Syringe Filter Units 0.22, trypsin-EDTA (0.25% trypsin; 0.1% EDTA), penicillin/streptomycin 100x, foetal bovine serum (FBS), Hank's balanced salt solution (HBSS), 1-µm and 8-µm pore size transwell™ inserts were bought from **Merck Millipore** (Burlington, MA, USA). Dimethyl sulfoxide (DMSO), paraformaldehyde (PFA), phalloidin-tetramethylrhodamine B isothiocyanate (phalloidin-TRITC), bovine serum albumin (BSA), fluoroshield™, sodium pyruvate solution 100 mM, resazurin sodium salt, Dulbecco's modified Eagle's Medium-high glucose (DMEM), phosphate buffered saline (PBS), N-(2-Hydroxyethyl)piperazine-N′-(2-ethanesulfonic acid) (HEPES) buffer solution, propranolol hydrochloride, primers, 2′,7′-Dichlorofluorescin diacetate (DCFH-DA), hydrogen peroxide (H_2O_2) solution, 6-Hydroxy-2,5,7,8-tetramethylchromane-2-carboxylic acid (Trolox), methanol, chloroform, acetic acid, sulfuric acid and ammonium acetate were obtained from **Sigma-Aldrich** (St. Louis, MO, USA).

IV.2. Methods

IV.2.1. Human faecal fermentation samples

Faecal samples obtained from five healthy donors who had not taken antibiotics in the past 6 months, were diluted in fermentation media (FM) with different carbon sources (commercial raftilose and microbial FOS) and incubated in anaerobic chambers for 12 and 24 h following the methodology used by Madureira et. al 2016[103]. The samples were also incubated in media without any carbon source as a control. The

products obtained from the fermentations were filtered (0.22-μm pore size) and diluted in MEM at 1:10, 1:6 and 1:3 volume ratios.

IV.2.2. Quantification of SCFA

The concentration of relevant SCFA (acetate, propionate, iso-butyrate and n-butyrate) in the fermentation medium was quantified by high performance liquid chromatography (HPLC). Briefly, the HPLC system was equipped with a Rezex ROA-Organic Acid H+ (300×7.8 mm) column from Phenomenex. Samples were eluted with sulfuric acid 2.5 mM, at a flow rate of 0.6 $mL \cdot min^{-1}$ and the run was carried out at 60 °C. The samples were eluted with an internal pattern (crotonic acid) and detected at 210 nm, being the average retention time of 16.30 min for formic acid, 17.95 min for acetic acid, 21.11 min for propionic acid, 23.92 min for iso-butyric acid and 25.90 min for n-butyric acid.

The area of the SCFA peaks in the samples was compared with the areas of calibration curves plotted using a series of standard solutions (**appendix A**). The concentration of SCFA was obtained after interpolation of the area of the samples according to the calibration curve.

IV.2.3. Cell culture

Cells were maintained in media with 100 $U \cdot mL^{-1}$ of penicillin and 100 $\mu g \cdot mL^{-1}$ of streptomycin (1% Pen/Strep), at 37 °C and in a 5% CO_2 atmosphere. Culture media was changed every 2-3 days and cells were routinely sub-cultured assuring a maximum confluence of 70-80%.

Co-cultures of Caco-2 and HT29-MTX cells were used to mimic the intestinal epithelium. The ratio of Caco-2 and HT29-MTX cells was 9:1 and the media used was MEM supplemented with 20% FBS and 1% sodium pyruvate. Cells were grown for 21 days and seeded on: Millicell® 12-well hanging inserts with polyethylene terephthalate (PET) membranes and, on 96 and 24-well plates. PET membranes with 1 and 8-μm pore sizes were used. The transwell membranes were used uncoated, coated with rat tail type-I collagen (50 $\mu g \cdot mL^{-1}$) or coated with a mixture of rat tail type-I collagen (50 $\mu g \cdot mL^{-1}$) and Matrigel™ (300 $\mu g \cdot mL^{-1}$). Briefly, 112 μL of the coating solution in cold serum-free MEM were added to each insert, incubated at 37 °C for 1-2h, followed by a PBS rinse.

IV.2.4. Metabolic activity

The resazurin reduction (**figure 29**) assay was used to determine the metabolic activity of cells.

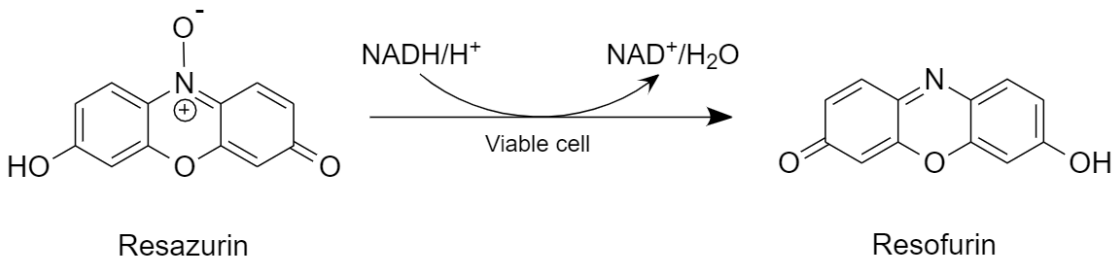

Figure 28: Reduction of low fluorescent oxidized blue dye resazurin to the fluorescent pink product resorufin. Created with ChemDraw.

Caco-2 cells were plated in 96-well plates at 1.1 x 10^4 cells·cm^{-2} per well. After 24h, the culture media (MEM) was removed and replaced by the fermentation products of human faecal samples diluted in MEM at different volume ratios (1:10, 1:6 and 1:3). After 24 or 48h, the media was removed and replaced with a 10 µg·mL^{-1} resazurin sodium salt solution in MEM.

Caco-2 and HT29-MTX cells were seeded in 96-well plates at 1.00 x 10^5 cells·cm^{-2} using 200 µL of cell suspension per well at a 9:1 ratio. After 21 days, the cell culture media (MEM) was removed and replaced by the products of fermentation of human faecal samples diluted in MEM at a 1:6 ratio. After 24h, the media was removed and replaced with a 10 µg·mL^{-1} resazurin sodium salt solution in MEM.

Fresh fermentation media (FM) was used as a vehicle control. MEM and DMSO (40% v/v) were used as positive and negative controls, respectively. Cell-free wells containing the 10 µg·mL^{-1} resazurin salt solution in MEM were used as blanks. The cell metabolic activity was determined by measuring the fluorescence of resofurin (λ_{ex}= 560 nm, λ_{em}= 590 nm) using a BioTeK® Synergy H1 (Winnoski, VT, USA) microplate reader. The results are expressed as a percentage of cell viability in relation to the positive control (untreated cells in MEM).

IV.2.5. Transepithelial electrical resistance (TEER)

The barrier integrity was assessed by measuring the trans-epithelial electrical resistance (TEER) using a Millicell® ERS-2 volt-ohmmeter (Merck Millipore, Billerica, MA, USA) and STX chopstick electrodes. The TEER (Ω·cm^2) was calculated by subtracting the readings of cell-free Millicell® inserts from the cell-cultured Millicell® inserts and multiplying by the surface area of the membrane (1.12 cm^2).

IV.2.6. Intestinal permeability assay

Propranolol hydrochloride was used to assess the transcellular transport of Caco-2/HT29-MTX co-cultures, grown on Millicell® 12-well hanging inserts. Cells were seeded at 1.00 x 10^5 cells·cm^{-2} using

200 or 500 µL of cellular suspension per well at a 9:1 ratio. After 21 days, the cell culture media (MEM) was removed and replaced by the test samples.

The transport media used was HBSS, pH 7.4 supplemented with 25 mM HEPES (HBSS-HEPES). A stock solution of propranolol was prepared in DMSO and diluted in HBSS-HEPES to final concentrations of 1% (v/v) DMSO and 50 or 100 µM propranolol. The propranolol solution was added to the apical chamber and the cells incubated at 37 °C under gentle agitation (100 rpm) for 4h. Samples were collected (500 µL) from the basolateral side at different time points (1h, 2h, 3h, and 4h) for analysis by HPLC and replenished with fresh HBSS. The TEER was measured throughout the experiment.

The amount of propranolol in the collected samples was quantified by HPLC. The LC system (UHPLC Agilent 1290 Infinity II) used was equipped with a Kinetex® LC column (2.6 µm XB-C18 100 Å) from Phenomenex. Samples were eluted with a mixture of acetonitrile and ammonium acetate 25 mM (pH = 3), at a flow rate of 1.0 mL·min^{-1} and the run was carried out at 4 °C. The samples were eluted and monitored with a Diode Array Detector (DAD, Agilent Technologies, Santa Clara, CA, USA) at 230 and 290 nm, being the retention time 7.7 min.

The area of the propranolol peak in the samples was compared with the areas of calibration curves plotted using a series of propranolol standards solutions prepared in HBSS-HEPES at concentrations ranging from 0.4 to 100 µM (**appendix B**). The concentration of propranolol was obtained after interpolation of the area of the samples in the calibration curve.

The apparent permeability coefficient (P_{app}, cm·s^{-1}) was calculated according to **equation 1.**,

$$P_{app} = \frac{dQ}{dt} \times \frac{V}{A \times C_0}$$

Equation 1

where $\frac{dQ}{dt}$ is the permeability rate (µM·s^{-1}), which corresponds to the slope of the cumulative increase in the concentration of propranolol in the basolateral chamber over time, V is the volume of the basolateral chamber (cm^3), A is the surface area of the insert (1.12 cm^2) and C_0 is the initial concentration of propranolol in the apical compartment (50 or 100 µM).

IV.2.7. Production of reactive oxygen species

The DCFH-DA reduction (**figure 30**) assay was used to determine the generation of reactive oxygen species (ROS) by the Caco-2/HT29-MTX co-culture.

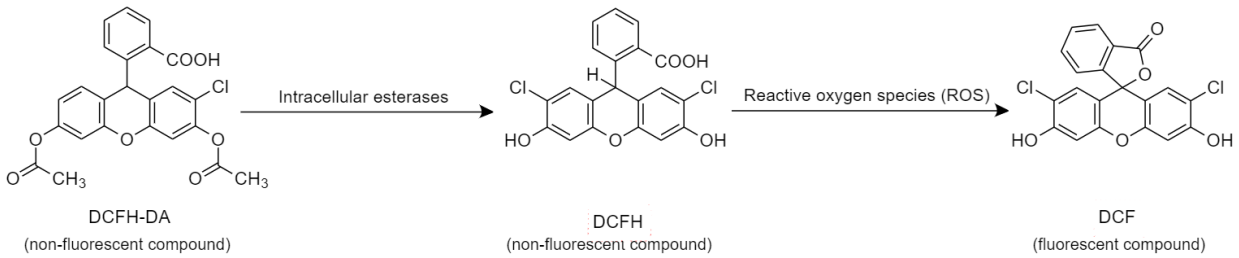

Figure 29:DCFH-DA deacetylation followed by DCFH oxidation. After diffusion into the cell, DCFH-DA is deacetylated by cellular esterases to a non-fluorescent compound, which is later oxidized by ROS into fluorescent dichlorofluorescein (DCF) allowing the assessment of ROS activity. Created with ChemDraw.

Cells were seeded in 96-well plates at 1.00 x 10^5 cells·cm^{-2} using 200 µL of cellular suspension per well at a 9:1 ratio. After 21 days, the cell culture media (MEM) was removed and replaced by 10 µM of DCFH-DA in HBSS. After 1h, the DCFH-DA solution was removed and replenished by the products of fermentation of human faecal samples diluted in MEM at a 1:6 ratio. After a 4h incubation at 37°C, the oxidative activity was determined by measuring the fluorescence of DCF. The protective effect of the samples was also determined. After 4h of incubation with samples, the media was removed and 2.5 mM H_2O_2 were added. After 1h, the protective effect was determined by measuring the fluorescence of DCF. Trolox (50 µg·mL^{-1}), an antioxidant compound analogue to vitamin E, and H_2O_2 (2.5 mM) were used as negative and positive controls respectively and incubated with cells during the first 4 hours[104].

The results are expressed in relation to the control (HBSS). The fluorescence of DCF (λ_{ex}= 495 nm, λ_{em}= 525 nm) was measured using a BioTeK® Synergy H1 (Winnoski, VT, USA) microplate reader.

IV.2.8. Inflammation activity assay

The cellular inflammatory response was determined by quantifying the secretion of IL-8 using the LEGEND MAX™ Human IL-8 ELISA Kit and the expression of *IL1B*, *IL6*, *CXCL8*, *TNF* and *PTGS2* genes by qRT-PCR.

Cells were seeded in 24-well plates at 1.00 x 10^5 cells·cm^{-2} using 500 µL of cell suspension per well at 9:1 ratio. After 21 days, the cell culture media (MEM) was removed and replaced by MEM supplemented (1:6) with human faecal fermentation products. MEM and 50 ng·mL^{-1} of TNF-α were used as negative and positive controls, respectively. After 4h of incubation, the supernatant was collected and store at -20 °C for later detection of IL-8 by the LEGEND MAX™ Human IL-8 ELISA Kit. The concentration of human IL-8 was obtained after interpolation of the absorbance (450-570nm) of the samples in the calibration curve (**appendix C**).

IV.2.8.1. RNA extraction and complementary DNA synthesis

Genomic DNA and total RNA were extracted from the cells using the AllPrep DNA/RNA Mini Kit. RNA concentration was measured using a NanoDrop™ 2000 spectrophotometer (Thermo Fisher Scientific). The RNA was reverse transcribed using the SuperScript™ VILO™ cDNA Synthesis Kit and a Veriti™ 96-Well Thermal Cycler.

IV.2.8.2. Quantitative polymerase chain reaction

Relative quantification of gene expression was performed using an Applied Biosystems™ StepOnePlus™ Real-Time PCR System (Thermo Fisher Scientific). The primer sequences (shown in **table 3**) were kindly shared by Dr. Maria del Carmén de Andrés, epigenetic unit leader at the Institute of Biomedical Research of A Coruña (INIBIC). Three housekeeping genes were initially tested (*ACTB, RPL13A, GAPDH*). A 20 µL reaction mixture was prepared in triplicate, containing 1 µL of complementary DNA, 10 µL of Power SYBR® Green PCR Master Mix and 1 µM of each primer.

Table 3: Forward (F) and reverse (R) primers used in the qPCR.

Gene	Abbreviation	Primer sequence (5'–3')
actin beta	*ACTB*	F: GGCATCCTCACCCTGAAGTA R: AGGTGTGGTGCCAGATTTTC
glyceraldehyde-3-phosphate dehydrogenase	*GADPH*	F: CCAGGTGGTCTCCTCTGACTTC R: TCATACCAGGAAATGAGCTTGACA
ribosomal protein L13	*RPL13A1*	F: AAAAAGCGGATGGTGGTTC R: CTTCCGGTAGTGGATCTTGG
interleukin 1 beta	*IL1B*	F: TGGCAATGAGGATGACTTGTTC R: CTGTAGTGGTGGTCGGAGATT
interleukin 6	*IL6*	F: GATGAGTACAAAAGTCCTGATCCA R: CTGCAGCCACTGGTTCTGT
C-X-C motif chemokine ligand 8	*CXCL8*	F: ACTGAGAGTGATTGAGAGTGGAC R: AACCCTCTGCACCCAGTTTTC
tumour necrosis factor	*TNF*	F: CCCAGGCAGTCAGATCATCTTC R: GGTTTGCTACAACATGGGCTACA
prostaglandin-endoperoxide synthase 2	*PTGS2* (v1)	F: GCTTTATGCTGAAGCCCTATGA R: ATCTGGCCGAGGCTTTTCTA
prostaglandin-endoperoxide synthase 2	*PTGS2* (v2)	F: CCTCAAGTCCCTGAGCATCAC R: CCTGTTTAAGCACATCGCATACT

Thermal cycler conditions included an initial activation step at 95 °C for 10 min, followed by a two-step PCR programme of 95°C for 10 s and 60°C for 60 s for 40 cycles. The $2^{-\Delta\Delta Ct}$ method was used for relative quantification of gene expression, and the data were normalized to the expression of β-actin and compared to the expression levels of untreated cells.

IV.2.9. Immunocytochemistry

Cells were fixed with cold methacarn (60% methanol, 30% chloroform, 10% acetic acid, % vol/vol) for 20 min at 4 °C. Cells were then washed with an aqueous solution of 3 % (v/v) acetic acid. The fixed cells were incubated with a 2% (w/v) BSA solution in PBS to minimise non-specific antibody bonding. After blocking, cells were incubated with 5 $\mu g \cdot mL^{-1}$ Alexa Fluor® 488 conjugated occludin monoclonal antibody (OC-3F10) and 0.1 $\mu g \cdot mL^{-1}$ phalloidin-TRITC overnight, at 4°C. Finally, and after extensive washes, cells were stained with 0.2 $\mu g \cdot mL^{-1}$ DAPI for 10 min and preserved in fluoroshield mounting media. Cells were imaged using a Zeiss LSM780 confocal laser scanning microscope (Oberkochen, Germany) and analysed using Zen 2010 software and ImageJ.

IV.2.10. Statistical analysis

Results are shown as Mean ± SD. The Shapiro-Wilk test was used to verify if the data followed a normal distribution. P-values were determined using a two-way analysis of variance (ANOVA) with Tukey's post-hoc test or the Student's t-test for independent samples. The statistical analysis was carried out using Graph Pad Prism 8.2.1 (San Diego, CA, USA).

References

1. Williams, C. F. *et al.* Comparative Analysis of Intestinal Tract Models. *Annu. Rev. Food Sci. Technol.* **6**, 329–350 (2015).

2. Cheng, L. K. *et al.* The gastrointestinal system. *Syst. Biol. Med.* **2**, 65–79 (2010).

3. Campbell, J., Berry, J. & Liang, Y. Shackelford's Surgery of the Alimentary Tract Anatomy and Physiology of the Small Intestine. in *Shackelford's Surgery of the Alimentary Tract* 817–841 (Elsevier Inc., 2019).

4. Meerveld, B. G.-V., Johnson, A. C. & Grundy, D. *Gastrointestinal Physiology and Function*. *Handbook of Experimental Pharmacology* **239**, (Springer International Publishing, 2017).

5. Azzouz, L. L. & Sharma, S. Physiology, Large Intestine. *StatPearls Publishing* (2018). Available at: https://www.ncbi.nlm.nih.gov/books/NBK507857/. (Accessed: 30th March 2019)

6. Dutton, J. S., Hinman, S. S., Kim, R., Wang, Y. & Allbritton, N. L. Primary Cell-Derived Intestinal Models: Recapitulating Physiology. *Trends in Biotechnology* **37**, 744–760 (2019).

7. Allaire, J. M. *et al.* The Intestinal Epithelium: Central Coordinator of Mucosal Immunity. *Trends Immunol.* **39**, 677–696 (2018).

8. Petersen, C. & Round, J. L. Defining dysbiosis and its influence on host immunity and disease. *Cell. Microbiol.* **16**, 1024–1033 (2014).

9. Danneskiold-Samsøe, N. B. *et al.* Interplay between food and gut microbiota in health and disease. *Food Res. Int.* **115**, 23–31 (2018).

10. Carding, S., Verbeke, K., Vipond, D. T., Corfe, B. M. & Owen, L. J. Dysbiosis of the gut microbiota in disease. *Microb. Ecol. Health Dis.* **26**, (2015).

11. Cani, P. D. *et al.* Microbial regulation of organismal energy homeostasis. *Nat. Metab.* **1**, 34–46 (2019).

12. Nicholson, J. K. *et al.* Host-gut microbiota metabolic interactions. *Science (80-.).* **336**, 1262–1267 (2012).

13. Valdes, A. M., Walter, J., Segal, E. & Spector, T. D. Role of the gut microbiota in nutrition and health. *BMJ* **361**, 36–44 (2018).

14. Abrahamson, M., Hooker, E., Ajami, N. J., Petrosino, J. F. & Orwoll, E. S. Successful collection of stool samples for microbiome analyses from a large community-based population of elderly men. *Contemp. Clin. Trials Commun.* **7**, 158–162 (2017).

15. Williams, G. M. *et al.* Gut microbiome analysis by post: Evaluation of the optimal method to collect stool samples from infants within a national cohort study. *PLoS One* **14**, (2019).

16. Pascale, A., Marchesi, N., Govoni, S., Coppola, A. & Gazzaruso, C. The role of gut microbiota in obesity, diabetes mellitus, and effect of metformin: new insights into old diseases. *Curr. Opin. Pharmacol.* **49**, 1–5 (2019).

17. Forster, S. C. *et al.* A human gut bacterial genome and culture collection for improved metagenomic analyses. *Nat. Biotechnol.* **37**, 186–194 (2019).

18. Louis, P., Hold, G. L. & Flint, H. J. The gut microbiota, bacterial metabolites and colorectal cancer. *Nat. Rev. Microbiol.* **12**, 661–672 (2014).

19. Leprun, P. M. B. & Clarke, G. The gut microbiome and pharmacology: a prescription for therapeutic targeting of the gut–brain axis. *Curr. Opin. Pharmacol.* **49**, 17–23 (2019).

20. Sommer, F. & Bäckhed, F. The gut microbiota-masters of host development and physiology. *Nat. Rev. Microbiol.* **11**, 227–238 (2013).

21. Zmora, N., Suez, J. & Elinav, E. You are what you eat: diet, health and the gut microbiota. *Nat. Rev. Gastroenterol. Hepatol.* **16**, 35–56 (2019).

22. Rothschild, D. *et al.* Environment dominates over host genetics in shaping human gut microbiota. *Nature* **555**, 210–215 (2018).

23. Oliphant, K. & Allen-Vercoe, E. Macronutrient metabolism by the human gut microbiome: Major fermentation by-products and their impact on host health. *Microbiome* **7**, 1–15 (2019).

24. Peng, L., He, Z., Chen, W., Holzman, I. R. & Lin, J. Effects of butyrate on intestinal barrier function in a Caco-2 cell monolayer model of intestinal barrier. *Pediatr. Res.* **61**, 37–41 (2007).

25. Van der Beek, C. M., Dejong, C. H. C., Troost, F. J., Masclee, A. A. M. & Lenaerts, K. Role of short-chain fatty acids in colonic inflammation, carcinogenesis, and mucosal protection and healing. *Nutr. Rev.* **75**, 286–305 (2017).

26. Venegas, D. P. *et al.* Short Chain Fatty Acids (SCFAs)-Mediated Gut Epithelial and Immune Regulation and Its Relevance for Inflammatory Bowel Diseases. *Front. Immunol.* **10**, 277 (2019).

27. Wong, J. M. W., Souza, R., Kendall, C. W. C., Emam, A. & Jenkins, D. J. A. Colonic Health: Fermentation and Short Chain Fatty Acids. *J. Clin. Gastroenterol.* **37**, 253–256 (2011).

28. Chambers, E. S., Preston, T., Frost, G. & Morrison, D. J. Role of Gut Microbiota-Generated Short-Chain Fatty Acids in Metabolic and Cardiovascular Health. *Curr. Nutr. Rep.* **7**, 198–206 (2018).

29. Ohira, H., Tsutsui, W. & Fujioka, Y. Are Short Chain Fatty Acids in Gut Microbiota Defensive Players for Inflammation and Atherosclerosis? *J. Atheroscler. Thromb.* **24**, 660–672 (2017).

30. Cani, P. Gut cell metabolism shapes the microbiome. *Science (80-.).* **357**, 548–549 (2018).

31. Byndloss, M. X., Pernitzsch, S. R. & Bäumler, A. J. Healthy hosts rule within : ecological forces shaping the gut microbiota. *Mucosal Immunol.* **11**, 1299–1305 (2018).

32. Marchesi, J. R. *et al.* The gut microbiota and host health: A new clinical frontier. *Gut* **65**, 330–339 (2016).

33. Buttó, L. F. & Haller, D. Dysbiosis in intestinal inflammation: Cause or consequence. *Int. J. Med. Microbiol.* **306**, 302–309 (2016).

34. Mu, Q., Kirby, J., Reilly, C. M. & Luo, X. M. Leaky gut as a danger signal for autoimmune diseases. *Front. Immunol.* **8**, 1–10 (2017).

35. Suez, J., Zmora, N., Segal, E. & Elinav, E. The pros, cons, and many unknowns of probiotics. *Nat. Med.* **25**, 716–729 (2019).

36. Hill, C. *et al.* The international scientific association for probiotics and prebiotics consensus statement on the scope and appropriate use of the term probiotic. *Nat. Rev. Gastroenterol. Hepatol.* **11**, 506–514 (2014).

37. Food and Agriculture Organization of the United Nations & World Health Organization. *Guidelines for the Evaluation of Probiotics in Food*. (2012).

38. Thomas, C. M. & Versalovic, J. Probiotic-host communication: Modulation of Host Signaling Pathways. *Gut Microbes* **13**, 148–163 (2010).

39. Lebeer, S., Vanderleyden, J. & De Keersmaecker, S. C. J. Host interactions of probiotic bacterial surface molecules: comparison with commensals and pathogens. *Nat. Rev. Microbiol.* **8**, 171–184 (2010).

40. Segers, M. E. & Lebeer, S. Towards a better understanding of *Lactobacillus rhamnosus* GG - host interactions. *Microb. Cell Fact.* **13**, 1–16 (2014).

41. Gibson, G. R. & Roberfroid, M. B. Dietary modulation of the human colonic microbiota: Introducing the concept of prebiotics. *J. Nutr.* **125**, 1401–1412 (1995).

42. Gibson, G. R., Probert, H. M., Loo, J. Van, Rastall, R. A. & Roberfroid, M. B. Dietary modulation of the human colonic microbiota: updating the concept of prebiotics. *Nutr. Res. Rev.* **17**, 259 (2004).

43. Markowiak, P., Śliżewska, K., Markowiak, P. & Śliżewska, K. Effects of Probiotics, Prebiotics, and Synbiotics on Human Health. *Nutrients* **9**, 1021 (2017).

44. Gibson, G. R. *et al.* Expert consensus document: The International Scientific Association for Probiotics and Prebiotics (ISAPP) consensus statement on the definition and scope of prebiotics. *Nat. Rev. Gastroenterol. Hepatol.* **14**, 491–502 (2017).

45. Nobre, C. *et al.* Process development for the production of prebiotic fructo-oligosaccharides by Penicillium citreonigrum. *Bioresour. Technol.* **282**, 464–474 (2019).

46. Davani-Davari, D. *et al.* Prebiotics: Definition, types, sources, mechanisms, and clinical applications. *Foods* **8**, (2019).

47. Nobre, C., Cerqueira, M. Â., Rodrigues, L. R., Vicente, A. A. & Teixeira, J. A. Production and Extraction of Polysaccharides and Oligosaccharides and Their Use as New Food Additives. in *Industrial Biorefineries and White Biotechnology* 653–679 (Elsevier, 2015).

48. Nobre, C. *et al.* Production of fructo-oligosaccharides by *Aspergillus ibericus* and their chemical characterization. *LWT* **89**, 58–64 (2018).

49. Nascimento, A. K. C., Nobre, C., Cavalcanti, M. T. H., Teixeira, J. A. & Porto, A. L. F. Screening of fungi from the genus Penicillium for production of β- fructofuranosidase and enzymatic synthesis of fructooligosaccharides. *J. Mol. Catal. B Enzym.* **134**, 70–78 (2016).

50. Castro, C. C., Nobre, C., De Weireld, G. & Hantson, A.-L. Microbial co-culturing strategies for fructo-oligosaccharide production. *N. Biotechnol.* **51**, 1–7 (2019).

51. Chen, Q. *et al.* A Novel Prebiotic Blend Product Prevents Irritable Bowel Syndrome in Mice by Improving Gut Microbiota and Modulating Immune Response. *Nutrients* **9**, (2017).

52. Bryk, G. *et al.* Effect of a combination GOS/FOS® prebiotic mixture and interaction with calcium intake on mineral absorption and bone parameters in growing rats. *Eur. J. Nutr.* **54**, 913–923 (2015).

53. Whelan, K., Efthymiou, L., Judd, P. A., Preedy, V. R. & Taylor, M. A. Appetite during consumption of enteral formula as a sole source of nutrition: the effect of supplementing pea-fibre and fructo-oligosaccharides. *Br. J. Nutr.* **96**, 350–356 (2006).

54. Frei, R., Akdis, M. & O'Mahony, L. Prebiotics, probiotics, synbiotics, and the immune system. *Curr. Opin. Gastroenterol.* **31**, 153–158 (2015).

55. Costa, J. & Ahluwalia, A. Advances and Current Challenges in Intestinal *in vitro* Model Engineering: A Digest. *Front. Bioeng. Biotechnol.* **7**, 144 (2019).

56. Ashammakhi, N. *et al.* Gut-on-a-chip: Current progress and future opportunities. *Biomaterials* **255**, (2020).

57. Pereira, C., Costa, J., Sarmento, B. & Araújo, F. Cell-based in vitro models for intestinal permeability studies. in *Concepts and Models for Drug Permeability Studies.* 57–81 (2016).

58. Lea, T. Caco-2 cell line. in *The Impact of Food Bioactives on Health: In Vitro and Ex Vivo Models* 103–111 (Springer, Cham, 2015).

59. Béduneau, A. *et al.* A tunable Caco-2/HT29-MTX co-culture model mimicking variable permeabilities of the human intestine obtained by an original seeding procedure. *Eur. J. Pharm. Biopharm.* **87**, 290–298 (2014).

60. Lesuffleur, T., Barbat, A., Dussaulx, E. & Zweibaum, A. Growth Adaptation to Methotrexate of HT-29 Human Colon Carcinoma Cells Is Associated with Their Ability to Differentiate into Columnar Absorptive and Mucus-secreting Cells. *Cancer Res.* **50**, (1990).

61. Lozoya-Agullo, I. *et al.* Usefulness of Caco-2/HT29-MTX and Caco-2/HT29-MTX/Raji B Coculture Models To Predict Intestinal and Colonic Permeability Compared to Caco-2 Monoculture. *Mol. Pharm.* **14**, 1264–1270 (2017).

62. Sarmento, B. *et al.* Cell-based in vitro models for predicting drug permeability. in *Concepts and Models for Drug Permeability Studies* 57–81 (2016).

63. Tibbitt, M. W. & Anseth, K. S. Hydrogels as extracellular matrix mimics for 3D cell culture. *Biotechnol. Bioeng.* **103**, 655–663 (2009).

64. Fatehullah, A., Tan, S. H. & Barker, N. Organoids as an *in vitro* model of human development and disease. *Nat. Cell Biol.* **18**, 246–254 (2016).

65. Kim, H. J., Li, H., Collins, J. J. & Ingber, D. E. Contributions of microbiome and mechanical deformation to intestinal bacterial overgrowth and inflammation in a human gut-on-a-chip. *Proc. Natl. Acad. Sci. U. S. A.* **113**, E7–E15 (2016).

66. Pearce, S. C. *et al.* Intestinal *in vitro* and *ex vivo* Models to Study Host-Microbiome Interactions and Acute Stressors. *Front. Physiol.* **9**, (2018).

67. Nissen, L., Casciano, F. & Gianotti, A. Intestinal fermentation in vitro models to study food-induced gut microbiota shift: an updated review. *FEMS Microbiol. Lett.* **367**, (2020).

68. Fritz, J. V, Desai, M. S., Schneider, J. G., Shah, P. & Wilmes, P. From meta-omics to causality: experimental models for human microbiome research. *Microbiome* **1**, 14 (2013).

69. Molly, K., Woestyne, M. Vande & Verstraete, W. Development of a 5-step multi-chamber reactor as a simulation of the human intestinal microbial ecosystem. *Appl. Microbiol. Biotechnol.* 254–258 (1993).

70. Van de Wiele, T., Van den Abbeele, P., Ossieur, W., Possemiers, S. & Marzorati, M. The Simulator of the Human Intestinal Microbial Ecosystem (SHIME®). in *The Impact of Food Bioactives on Health* 305–317 (Springer International Publishing, 2015). doi:10.1007/978-3-319-16104-4_27

71. Anson, N. M. *et al.* Bioprocessing of Wheat Bran Improves in vitro Bioaccessibility and Colonic Metabolism of Phenolic Compounds. *J. Agric. Food Chem.* **57**, 6148–6155 (2009).

72. Minekus, M. The TNO Gastro-Intestinal Model (TIM). in *The Impact of Food Bioactives on Health* 37–46 (2015).

73. Minekus, M., Marteau, P., Havenaar, R. & Veld, J. H. J. H. A Multicompartmental Dynamic Computer- controlled Model Simulating the Stomach and Small Intestine. *Altern. to Lab. Anim.* 197–209 (1995).

74. Marzorati, M. *et al.* The HMI™ module: a new tool to study the Host-Microbiota Interaction in the human gastrointestinal tract in vitro. *BMC Microbiol.* **14**, 133 (2014).

75. Shah, P. *et al.* A microfluidics-based in vitro model of the gastrointestinal human-microbe interface. *Nat. Commun.* **7**, (2016).

76. Shah, P. *et al.* A microfluidics-based in vitro model of the gastrointestinal human–microbe interface. *Nat. Commun.* **7**, 11535 (2016).

77. García-Villalba, R. *et al.* Gastrointestinal Simulation Model TWIN-SHIME Shows Differences between Human Urolithin-Metabotypes in Gut Microbiota Composition, Pomegranate Polyphenol Metabolism, and Transport along the Intestinal Tract. (2017).

78. Yin, N. *et al.* Variability of arsenic bioaccessibility and metabolism in soils by human gut microbiota using different in vitro methods combined with SHIME. *Sci. Total Environ.* **566–567**, 1670–1677 (2016).

79. Sivieri, K. *et al. Lactobacillus acidophilus* CRL 1014 improved "gut health" in the SHIME®reactor. *BMC Gastroenterol.* **13**, 100 (2013).

80. Nobre, C., Gonçalves, D. A., Teixeira, J. A. & Rodrigues, L. R. One-step co-culture fermentation strategy to produce high-content fructo-oligosaccharides. *Carbohydr. Polym.* **201**, 31–38 (2018).

81. Huh, D., Hamilton, G. A. & Ingber, D. E. From 3D cell culture to organs-on-chips. *Trends Cell Biol.* **21**, 745–754 (2011).

82. Chung, H. H., Mireles, M., Kwarta, B. J. & Gaborski, T. R. Use of porous membranes in tissue barrier and co-culture models. *Lab Chip* **18**, 1671–1689 (2018).

83. Liberio, M. S., Sadowski, M. C., Soekmadji, C., Davis, R. A. & Nelson, C. C. Differential effects of tissue culture coating substrates on prostate cancer cell adherence, morphology and behavior. *PLoS One* **9**, (2014).

84. Frantz, C., Stewart, K. M. & Weaver, V. M. The extracellular matrix at a glance. *J. Cell Sci.* **123**, 4195–4200 (2010).

85. Hughes, C. S., Postovit, L. M. & Lajoie, G. A. Matrigel: a complex protein mixture required for optimal growth of cell culture. *Proteomics* **10**, 1886–1890 (2010).

86. Chen, X. M., Elisia, I. & Kitts, D. D. Defining conditions for the co-culture of Caco-2 and HT29-MTX cells using Taguchi design. *J. Pharmacol. Toxicol. Methods* **61**, 334–342 (2010).

87. Gao, Y. *et al.* Modulation of intestinal epithelial permeability in differentiated caco-2 cells exposed to aflatoxin M1 and ochratoxin a individually or collectively. *Toxins (Basel).* **10**, (2018).

88. Araújo, F. *et al.* In vitro M-like cells genesis through a tissue-engineered triple-culture intestinal model. *J. Biomed. Mater. Res. - Part B Appl. Biomater.* **104**, 782–788 (2016).

89. Lechanteur, A., Almeida, A. & Sarmento, B. Elucidation of the impact of cell culture conditions of Caco-2 cell monolayer on barrier integrity and intestinal permeability. *Eur. J. Pharm. Biopharm.* **119**, 137–141 (2017).

90. Srinivasan, B. *et al.* TEER Measurement Techniques for In Vitro Barrier Model Systems. *J. Lab. Autom.* **20**, 107–126 (2015).

91. Stockdale, T. P., Challinor, V. L., Lehmann, R. P., De Voss, J. J. & Blanchfield, J. T. Caco-2 Monolayer Permeability and Stability of *Chamaelirium luteum* (False Unicorn) Open-Chain Steroidal Saponins. *ACS Omega* **4**, 7658–7666 (2019).

92. Corning. Transwell® Permeable Supports. *Transwell Premeable Support* 1–9 (2017).

93. Casillo, S. M., Peredo, A. P., Perry, S. J., Chung, H. H. & Gaborski, T. R. Membrane Pore Spacing Can Modulate Endothelial Cell-Substrate and Cell-Cell Interactions. *ACS Biomater. Sci. Eng.* **3**, 243–248 (2017).

94. Pham, V. T. *et al.* The effects of fermentation products of prebiotic fibres on gut barrier and immune functions *in vitro*. *PeerJ* **2018**, (2018).

95. National Center for Biotechnology Information. PubChem Database. Propranolol, CID=4946. Available at: https://pubchem.ncbi.nlm.nih.gov/compound/Propranolol (accessed on Mar. 26, 2020).

96. Brueckner, F. *et al.* Structure of β-adrenergic receptors. in *Methods in Enzymology* **520**, 117–151 (Academic Press Inc., 2013).

97. Ishida-Ishihara, S. *et al.* Osmotic gradients induce stable dome morphogenesis on extracellular matrix. *J. Cell Sci.* **133**, (2020).

98. Zweibaum, A., Laburthe, M., Grasset, E. & Louvard, D. Use of Cultured Cell Lines in Studies of Intestinal Cell Differentiation and Function. *Compr. Physiol.* (2011).

99. Vinolo, M. A. R., Rodrigues, H. G., Nachbar, R. T. & Curi, R. Regulation of inflammation by short chain fatty acids. *Nutrients* **3**, 858–876 (2011).

100. Alexander, C., Swanson, K. S., Fahey, G. C. & Garleb, K. A. Perspective: Physiologic Importance of Short-Chain Fatty Acids from Nondigestible Carbohydrate Fermentation. *Adv. Nutr.* **10**, 576–589 (2019).

101. Hung, T. Van & Suzuki, T. Short-Chain Fatty Acids Suppress Inflammatory Reactions in Caco-2 Cells and Mouse Colons. *J. Agric. Food Chem.* **66**, 108–117 (2018).

102. O'Hara, A. M. *et al.* Tumor necrosis factor (TNF)-α-induced IL-8 expression in gastric epithelial cells: Role of reactive oxygen species and AP endonuclease-1/redox factor (Ref)-1. *Cytokine* **46**, 359–369 (2009).

103. Madureira, A. R. *et al.* Fermentation of bioactive solid lipid nanoparticles by human gut microflora. *Food Funct.* **7**, 516–529 (2016).

104. National Center for Biotechnology Information. PubChem Compound Summary for CID 40634, Trolox. (2020). Available at: https://pubchem.ncbi.nlm.nih.gov/compound/Trolox. (Accessed: 26th April 2020)

105. Halliwell, B. & Whiteman, M. Measuring reactive species and oxidative damage *in vivo* and in cell culture: how should you do it and what do the results mean? *Br. J. Pharmacol.* **142**, 231–255 (2004).

Appendixes and Annexes

Appendix A: Standard curves used to calculate SCFAs concentration

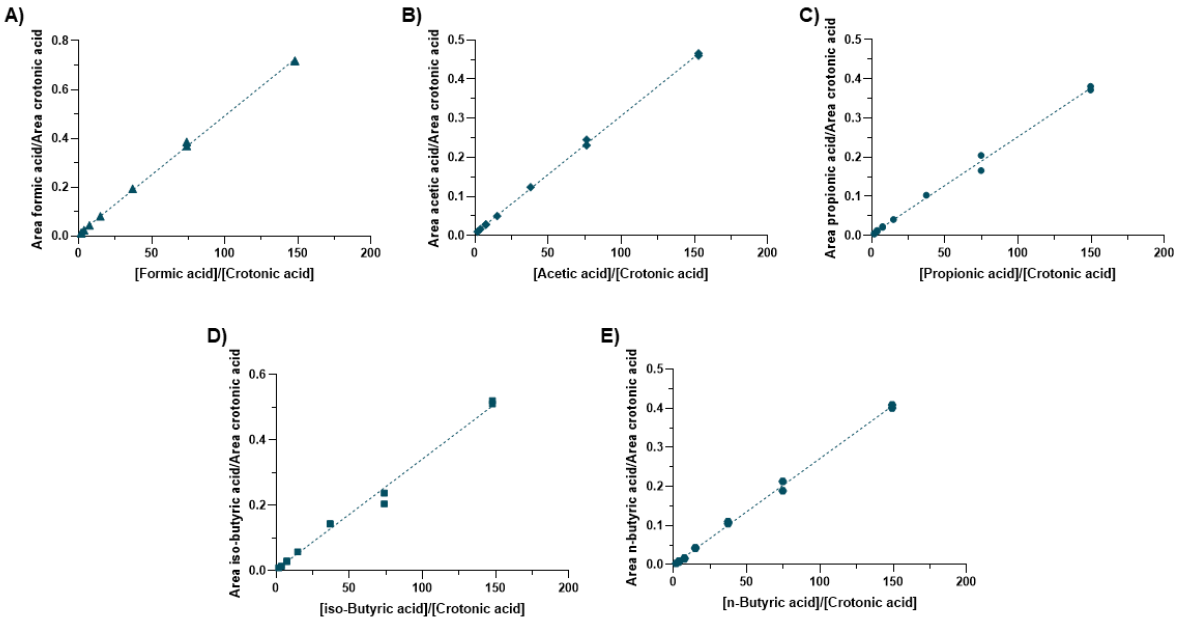

Appendix A: **SCFAs propranolol standard curve** obtained by the analysis of formic, acetic, propionic, iso-butyric and n-butyric acid standards. The peak area of the standard (AS) divide by the peak area of the internal pattern- crotonic acid (AP)- was plotted against the respective concentration of the standard ([S]) divided by the concentration of the internal pattern ([P]). The results were fitted to linear regressions (R^2 = 1.00) to obtain the equations (A) Formic acid: AS/AP = 0.0048 [S]/[P] + 0.0.0091 (B) Acetic acid: AS/AP = 0.0030 [S]/[P] + 0.0.0059 (C)Propionic acid: AS/AP = 0.0025 [S]/[P] + 0.0.0032 (D) iso-Butyric acid: AS/AP = 0.0034 [S]/[P] + 0.0.0026 (E) n-Butyric acid: AS/AP = 0.0027 [S]/[P] - 0.0.0005.

Appendix B: Standard curves used to calculate propranolol concentration

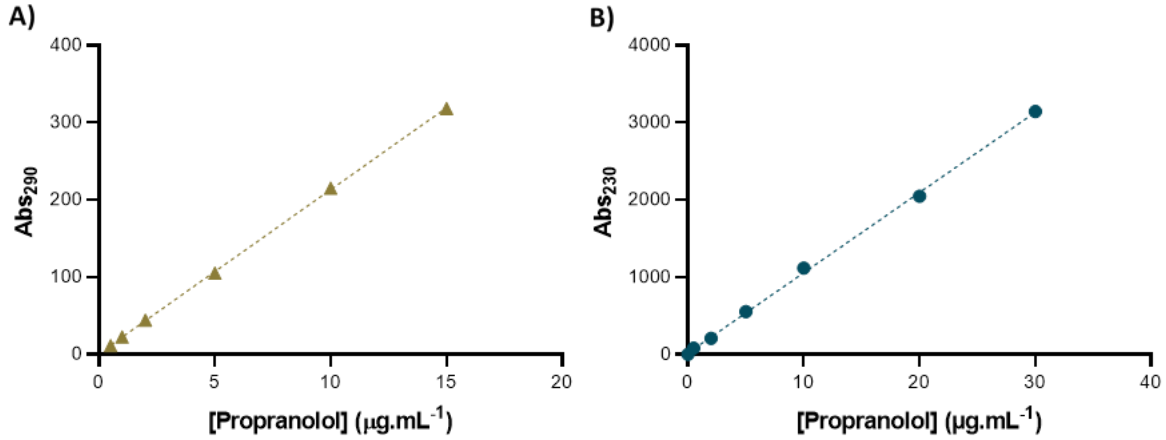

Appendix B: **HPLC propranolol standard curve** obtained by the analysis of propranolol standards in the range of (A) 0.5 - 15 µg.mL^{-1} (B) 0.5 - 30 µg.mL^{-1}. The peak area for each standard was plotted against its respective concentration of propranolol. The results were fitted to linear regressions (R^2 = 1.00) to obtain the equations (A) Abs_{290nm} = 21.2 [Propranolol] (µg.mL^{-1}) + 0.973 (B) Abs_{230nm} = 103.89 [Propranolol] (µg.mL^{-1}) + 17.98.

Appendix C: Standard curve used to calculate human IL-8 concentration

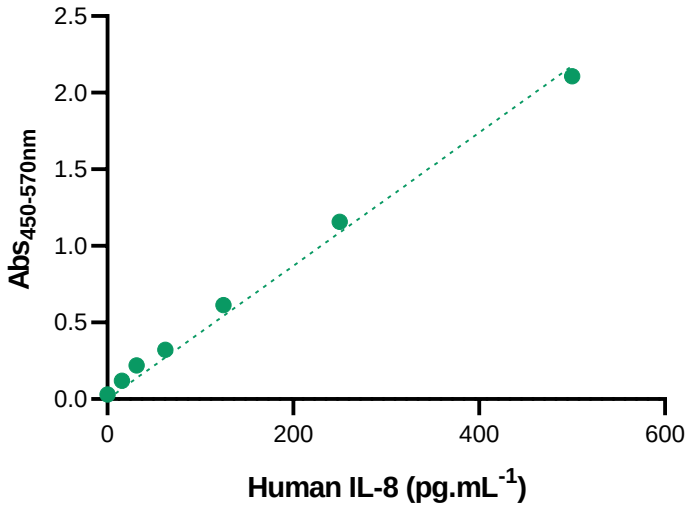

Appendix C: **Human IL-8 standard curve** obtained by the analysis of human IL-8 standards in the range of 0 - 500 pg.mL^{-1}. The absorbance 450-570nm for each standard was plotted against its respective concentration of human IL-8. The results were fitted to a linear regression (R^2 = 1.00) to obtain the equation $Abs450\text{-}570_{nm}$ = 0.0043 [Human IL-8] (µg.mL^{-1}).

Appendix D: TEER of Caco-2/HT29-MTX co-cultures during the intestinal permeability assay

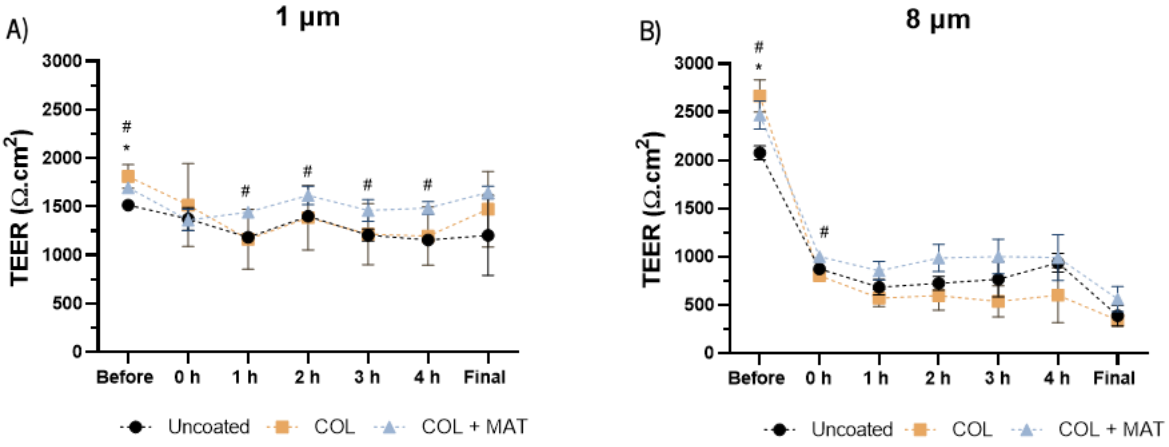

Appendix D: **Trans-epithelial electrical resistance (TEER) of Caco-2/HT29-MTX co-cultures during the intestinal permeability assay**. During 4 h, TEER was measured on (A) 1 µm and (B) 8 µm pore size Millicell® hanging inserts used uncoated or coated with collagen (COL) or collagen plus matrigel (COL + MAT). Millicell® inserts without coatings (Uncoated) were used as controls. Values show Mean ± SD (N≥2; *, $^{\#}p < 0.05$ vs control (Uncoated) with p-values obtained using the Student's t-test for independent samples). *p: COL and $^{\#}$p: COL + MAT.

Appendix E: Effect of ECM coatings on the cumulative fraction of propranolol transported

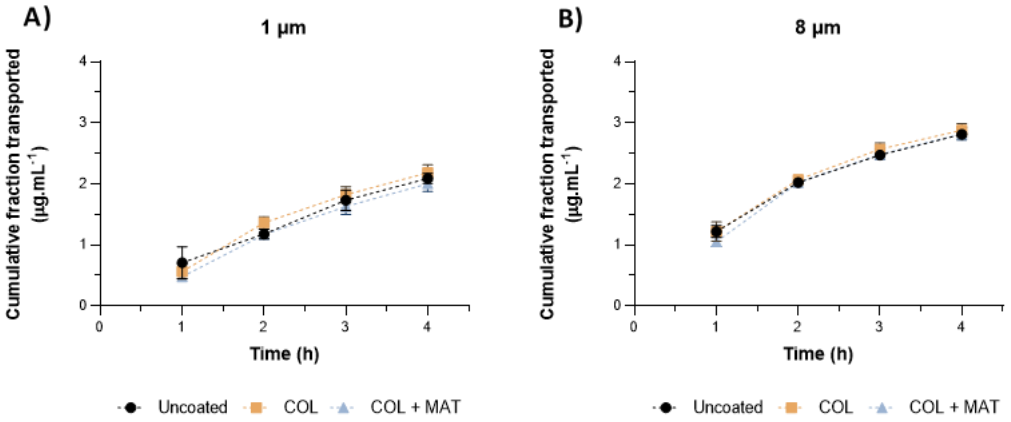

Appendix E: Cumulative fraction of propranolol transported across a Caco-2/HT29-MTX co-culture from the apical to the basolateral chamber of a transwell™ system. Cells were grown on (A) 1 µm and (B) 8 µm pore size Millicell® hanging inserts coated with collagen (COL) or a collagen and matrigel mix (COL + MAT). Millicell® inserts without coatings (Uncoated) were used as controls. Values show Mean ± SD (N≥3).

Appendix F: Effect of membrane pore size on the apparent permeability of propranolol

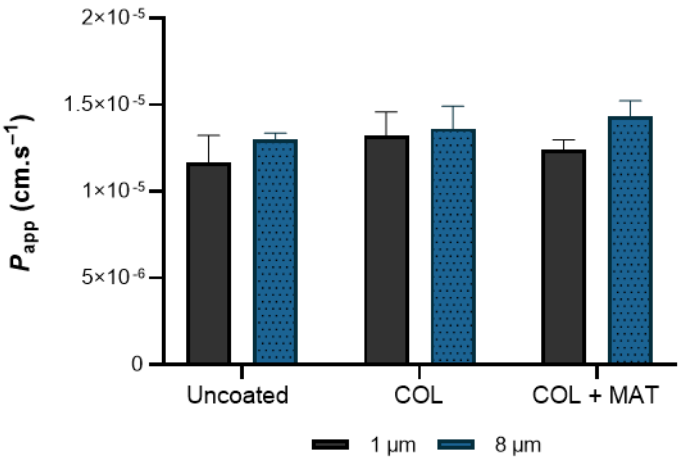

Appendix F: Apparent permeability of propranolol across a Caco-2/HT29-MTX co-culture culture from the apical to the basolateral chamber of a transwell™ system. Cells were grown on (A) 1 µm and (B) 8 µm pore size Millicell® hanging inserts coated with collagen (COL) or a collagen and matrigel mix (COL + MAT). Millicell® inserts (E) without coatings (Uncoated) were used as controls. Values show Mean ± SD (N=3).

Appendix G: TEER of Caco-2/HT29-MTX co-cultures during the differentiation process (21 days)

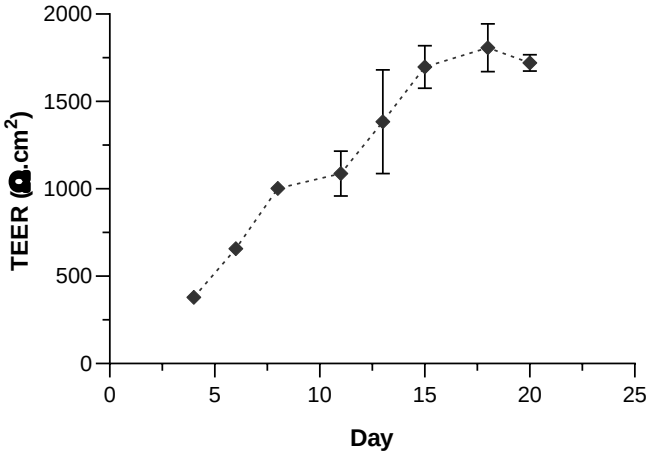

Appendix G: Trans-epithelial electrical resistance (TEER) of Caco-2/HT29-MTX co-cultures grown for 21 days on the apical side of 1 µm pore size Millicell® hanging inserts. Values show Mean ± SD (N=4; from 1 independent assay).

Appendix H: Cumulative fraction of propranolol transported across a Caco-2/HT29-MTX co-culture exposed to human faecal fermentation products

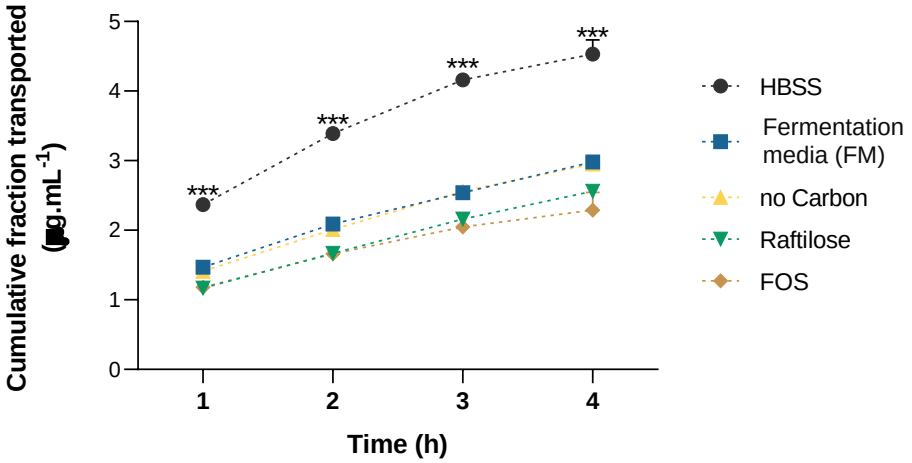

Appendix H: Cumulative fraction of propranolol transported across a Caco-2/HT29-MTX co-culture exposed to fermentation media (FM) or human faecal fermentation products from the apical to the basolateral chamber of a transwell™ system. Cells were grown on 1 µm pore size Millicell® hanging inserts used uncoated. Values show Mean ± SD (N≥2; ***p < 0.001 vs control (HBSS) with p-values obtained using the Student's t-test for independent samples that followed a normal distribution according to the Shapiro-Wilk test).

Appendix I: Relative expression of *CXCL8, TNF, IL1B* and *PTGS2* by Caco-2/HT29-MTX co-cultures normalized to the expression of *RPL13A1* gene

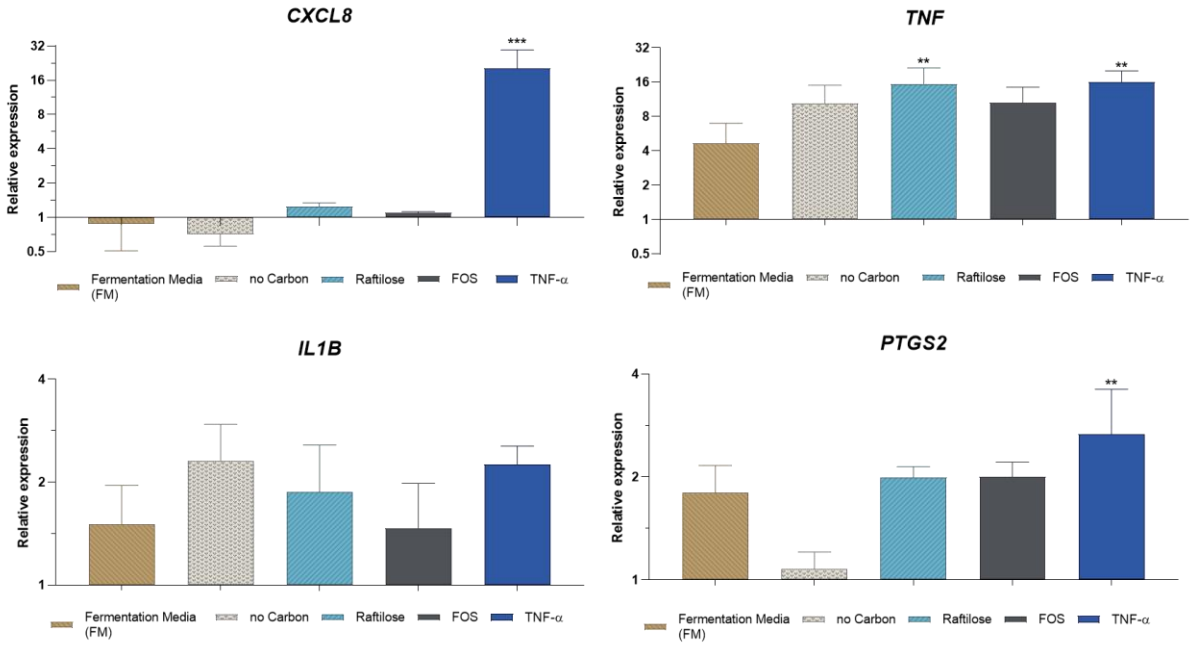

Appendix I: **Relative expression of *CXCL8*, *TNF*, *IL1B* and *PTGS2* by Caco-2/HT29-MTX co-cultures** exposed to MEM (negative control), 50 ng·mL^{-1} TNF-α (positive control), fermentation media (FM), products of fermentation of human faecal samples in media with no carbon source (no Carbon), with raftilose (Raftilose) or fructo-oligosaccharides (FOS), diluted in MEM (dilution 1:6), for 4h. Total RNA was extracted from the cells and reverse transcribed. The $2^{-\Delta\Delta Ct}$ method was used for relative quantification of gene expression, and the data were normalized to the expression of *RPL13A1* and compared to the expression levels of untreated cells. Values show Mean ± SD (N=3 from 3 independent assays; *p < 0.05; **p < 0.01 vs control (MEM); $^{\#}$p<0.05, $^{\#\#}$p<0.01 vs TNF- α p-values obtained using a one-way analysis of variance (ANOVA) with Tukey's post-hoc test for samples that followed a normal distribution according to the Shapiro-Wilk test).

Annex 1: Optimization of the production of reactive oxygen species assay

In order to verify if the fermentation products of faecal samples had a protective effect against an oxidative stimulus, H_2O_2 was used as an oxidant agent. For this, following the 4h incubation with the test samples, the media was removed and 2.5mM of H_2O_2 was added for an additional hour. Trolox, a known antioxidant compound, was used as a negative control on the first 4h incubation period.

Annex 1 shows that faecal samples grown in the presence of raftilose and FOS have a significant ($p<0.001$) increase on the production of ROS after incubation with H_2O_2. However, the samples that had a higher oxidative activity, the fermentation media and the no Carbon conditions, show no increase on the production of ROS.

The presence of intracellular ROS was assessed by the DCFH-DA assay where after diffusion into the cell, DCFH-DA is deacetylated by cellular esterases to a non-fluorescent compound (DCFH), which is later oxidized by ROS into dichlorofluorescein (DCF) which is easily detected by fluorescence. However, DCFH and DCF can diffuse out of cells and undergo extracellular reactions[105]. Before the addition of H_2O_2, samples were removed and with it all the DCF that had leaked out of the cells. Consequently, the results in **annex 1** show only the effect of the 1h incubation with H_2O_2.

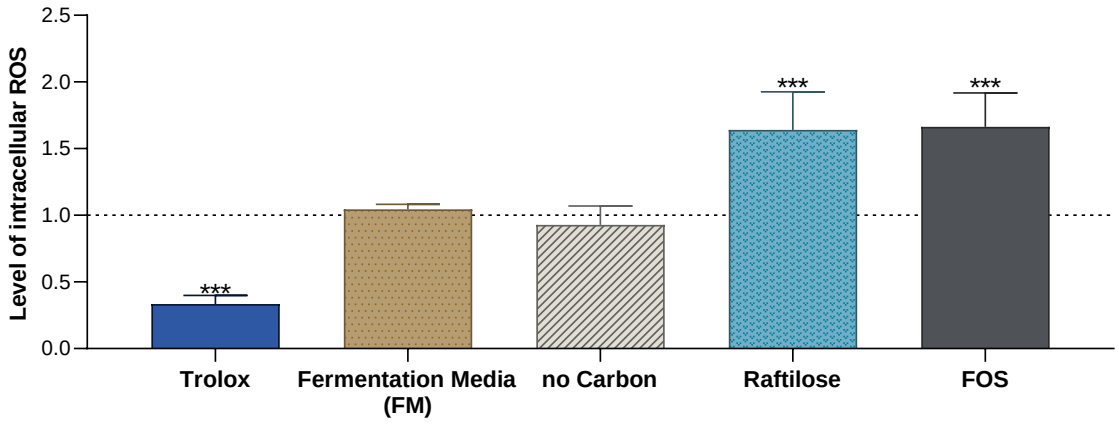

Annex 1: Production of ROS by Caco-2/HT29-MTX co-cultures exposed to human faecal fermentation products after incubation with H_2O_2. Caco-2/HT29-MTX co-culture production of ROS incubated for 1h with DCFH-DA and after its removal HBSS supplemented (1:6) with the fermentation media (FM) or products of fermentation of human faecal samples in with no carbon source (no Carbon), raftilose (Raftilose) or fructo-oligosaccharides (FOS) was added for 4h. HBSS was removed and cells were then incubated for 1h with H_2O_2. Trolox was used as a negative control. The production of ROS was determined by measuring the fluorescence of DCF (λex= 495 nm, λem= 525 nm) from the DCFH-DA reduction assay. Values show Mean ± SD (N=8 from 2 independent assays; ***$p < 0.001$ vs control (HBSS - dotted line at 1) p-values obtained using a two-way analysis of variance (ANOVA) with Tukey's post-hoc test for samples that followed a normal distribution according to the Shapiro-Wilk test).

In the future, it is advisable to add DCFH-DA only after the incubation with samples or H_2O_2. This way, there is less time for the DCFH and DCF to leak out of the cells. Please note that if DCFH and DCF leak out of the cells, extracellular reactions could happen and there could be measuring not only the light emission from the cells but also from the media.